ELSEVIER

New Astronomy 1 (1996) 271–297

NEW ASTRONOMY

# Molecular hydrogen in the central regions of southern infrared galaxies

Jan Koornneef[a,1,2], Frank P. Israel[b]

[a]*Kapteyn Institute & /S/[RON]/ Laboratory for Space Research, Postbus 800, 9700 AV Groningen, The Netherlands*
[b]*Sterrewacht, Postbus 9513, 2300 RA, Leiden, The Netherlands*

Received 8 March 1996; accepted 20 May 1996
Communicated by F. Duccio Macchetto

**Abstract**

An extensive set of molecular hydrogen observations of centers of southern infrared galaxies is presented. Our data are combined with published infrared and radio observations to investigate the relationship between nuclear and circumnuclear activity. We convert the observational data to absolute luminosities, by applying the known distances. The resulting dataset covers several decades in luminosity for the various parameters, which observe fairly tight correlations. The parameters of our (power law) fits are, at the level of accuracy achieved, not dependent on the type of nuclear activity: while the dataset comprises a mixture of alleged Seyfert, Liner & starburst galaxies, single fits match the complete sample well enough. In particular, non-thermal nuclei (AGN) present in some of the galaxies in the current sample, do not stand out in the parameters we investigated. The absence of a significant dependence on the nuclear type is consistent with the idea that the ever present starbursts energetically dominate a possible 'AGN in a dusty environment'-component in most galaxy nuclei with infrared excesses.

The size of the $H_2$ emitting region is found to be proportional to the square root of the 21 cm radio continuum luminosity. The excitation of the circumnuclear $H_2$ is dominated by shocks. If the $H_2$ extent marks the size of an inner cavity in the dense molecular material surrounding a galaxy nucleus and the radio luminosity is proportional to the mechanical luminosity of (circum)nuclear winds. This result then indicates that the cavity size occurs at constant pressure in the sample galaxies, in accordance with the superwind model by Heckman et al. (1990) [ApJS, 74, 833]. Our results, together with those obtained by others, thus suggest that luminosities and size scales of excited gas associated with active nuclei are dominated by the mechanical energy input. Given the difficulties of uniquely establishing the presence of an AGN, we cannot exclude that (a large fraction of the) infrared luminous galaxies procure part of their radiated energy through accretion onto a massive dark object.

*PACS:* 11.01.2; 11.09.4; 11.14.1; 11.19.3; 13.09.4
*Keywords:* Galaxies: active; Galaxies: ISM; Galaxies: nuclei; Galaxies: starburst; Infrared: ISM: lines and bands

[1]Based on observations collected at the European Southern Observatory (ESO) at La Silla, Chile.
[2]E-mail: koornneef@sron.rug.nl


*PII* S1384-1076(96)00011-5

## 1. Introduction

Following the initial detection of the 1–0 S(1) transition at 2.121 $\mu$m from molecular hydrogen ($H_2$) in the Seyfert galaxy NGC 1068 (Thompson et al., 1978), this transition was also detected in infrared-luminous IRAS 'starburst' galaxies, as well as in a plethora of galaxies with lower infrared luminosities. For a recent compilation of relevant data on Seyfert and starburst galaxies, we refer to Mouri & Taniguchi (1992), and references therein.

The importance of the near-infrared spectral regime for the study of starburst regions can be readily illustrated by referring to several recent papers on the well studied starburst galaxy NGC 253. Forbes et al. (1993) show that the spatial distributions of the Br $\gamma$, [FeII], and $H_2$, as well as the 2 $\mu$m & 6 cm continuum, are quite similar. The same is true for 12 $\mu$m (Piña et al., 1992). Differences in the spatial distributions become striking only at resolutions much better than 6 arcsec (or approximately 50 pc), and the $H_2$ emission is then seen to be more whispy. Also, on that scale Sams et al. (1994) find significant displacements between peaks in J, H, and K-band images, which they ascribe to uneven extinction to the central source(s). The correlation between the 2.2 and 10.8 $\mu$m images is much better, confirming that spatial extinction variations at these wavelengths are much less of a problem.

In contrast, optical and ultraviolet studies are handicapped by complex extinction and scattering effects due to the large amounts of dust usually present in and around galactic nuclei. As a result, the location and extent of the energy generating regions are obfuscated. For example, Muñoz-Tuñon et al. (1993) derive in their optical emission line study of NGC 253 a much *larger* star formation region than observed by us. This could mean that they see the outflow, rather than the actual star forming region. If a superwind interacts with cooler and denser material in the outflow cone, H$\alpha$, [NII] & [SII] emission lines are formed (see, e.g., Shull & Draine, 1987). The observed asymmetry of the velocity profiles (Fig. 1a of Muñoz-Tuñon et al., 1993) can then be interpreted in terms of an angle between the line of sight and the axis of the outflow cone[3]. Additionally, scattering of the light might be expected to affect the observed spatial distribution of the line emissions.

Nevertheless, when the obscuration characteristics of the line forming regions are well understood, optical line emission studies can provide powerful diagnostics (e.g., Mouri et al., 1989). In their study of [OI] 6300 Å emissions, Mouri et al. effectively corrected for extinction by plotting [OI]/H$\alpha$ vs. $H_2$ 1–0 S(1)/Br$\gamma$, and found that a single linear relationship exists for both AGN (Seyfert) & SBN (starburst) galaxies[4]. Analogously, Forbes & Ward (1993) find a strong correlation between the 1.644 $\mu$m [FeII] emission with the 6 cm radio continuum for a sample of, sometimes heavily obscured, active nuclei which includes SBNs, LINERs, & Seyfert's. This correlation does not show any obvious trend with nuclear activity type, and exists without extinction corrections.

Our own sample of southern galaxies was defined to be a subset of IRAS galaxies. We required that they were listed as IRAS *point sources* with a minimum 12 $\mu$m flux density of 1 Jy. In nearby galaxies, such strong and unresolved 12 $\mu$m IRAS emission characteristically originates in the nucleus, and is indicative of some type of nuclear activity. For these systems, confusion with strong emission from a galactic disk is unlikely, as this would be spatially resolved. In more distant galaxies, these same selection rules discriminate effectively against a disk origin of the observed 12 $\mu$m flux density, due to the luminosity constraint implied by our lower limit for the 12 $\mu$m flux density. Consistent with this semi-empirical argument is that, in a preliminary attempt, we found that the correlation between integrated CO luminosities and IRAS 12 $\mu$m luminosities is considerably better than between CO and 100 $\mu$m luminosities. Also relevant in this context are the findings of Giuricin et al. (1994).

[3]The data suggest that the inclination of the major axis of NGC 253 is roughly half the opening angle of the outflow cone; also see Heckman et al. (1990): their Table 6.

[4]In their sample, as in ours, NGC 6240 is outside of the relationship due to its exceedingly high $H_2$/Br$\gamma$ ratio.

They used the ratio of small-aperture 10 $\mu$m fluxes to IRAS 12 $\mu$m fluxes to derive the degree of compactness of the mid-infrared emission from galactic nuclei. Especially for high-luminosity sources, the degree of compactness is high enough that a very significant fraction of the IRAS 12 $\mu$m emission is concentrated in an aperture of order 6″ across. We have included their compactness values in Table 1. For all the galaxies in our dataset we obtained $H_2$ 1–0 S(1) line observations, with positive detections in the majority of cases.

In this paper, we present the results of our investigation. For a subset of galaxies, we also measured other $H_2$ K-band transitions, in order to

Table 1
IRSPEC 1–0 S(1) $H_2$ line and continuum observations of southern galactic nuclei

| Galaxy | Continuum[a] 2.1 $\mu$m $10^{-17}$ W cm$^{-2}$ $\mu$m$^{-1}$ | 1–0 S(1) 2.121 $\mu$m $10^{-21}$ W cm$^{-2}$ | 1–0 S(1) Eq. width Å | Compactness[h] C | Note |
|---|---|---|---|---|---|
| NGC 253 | 1.06 | 6.9 ±0.4 | 6.5±0.4 | 0.43 | b |
| NGC1097 | 0.33 | < 0.4 | < 1.0 | 0.03 | |
| NGC1097N | 0.22 | 1.0 ±0.3 | 5.0±2.0 | | c |
| NGC1365 | 0.99 | 0.8 ±0.25 | 0.8±0.3 | 0.11 | |
| NGC1792 | 0.14 | 0.6 ±0.25 | 4.0±2.0 | | |
| NGC1808 | 0.94 | 2.6 ±0.6 | 2.8±0.7 | 0.87 | |
| NGC2369 | 0.15 | 0.8 ±0.35 | 5.0±2.0 | | |
| NGC2559 | 0.23 | 0.8 ±0.4 | 4.0±2.0 | | |
| He2-10 | 0.27 | 1.2 ±0.25 | 4.4±0.9 | | d |
| NGC2992 | 0.37 | 1.15±0.5 | 3.0±1.0 | 0.57 | |
| IC2554 | 0.15 | 0.9 ±0.3 | 6.0±2.0 | | |
| NGC3175 | 0.17 | 1.0 ±0.25 | 6.0±1.5 | | |
| NGC3256 | 0.38 | 3.8 ±0.4 | 10.0±1.1 | 0.85 | b |
| NGC3281 | 0.10 | 1.0 ±0.4 | 10.0±4.0 | | |
| NGC3783 | 0.46 | 0.8 ±0.3 | 2.0±1.0 | 0.90 | |
| NGC4038 | – | 1.0 ±0.4 | – | – | |
| NGC4527 | 0.48 | < 0.2 | < 1.0 | 0.06 | |
| NGC4666 | 0.31 | < 0.35 | < 1.0 | | |
| NGC4835 | 0.07 | < 0.4 | < 6.0 | | |
| NGC4945 | 0.82 | 12.9 ±0.5 | 15.7±0.6 | 0.07 | b,e |
| NGC5128 | 1.73 | 4.7 ±0.2 | 2.7±0.2 | | f |
| NGC5188 | – | 0.8 ±0.35 | – | 0.42 | |
| NGC5236 | 0.69 | 3.1 ±0.3 | 4.5±0.5 | 0.01 | b |
| NGC5253 | – | 1.5 ±0.4 | – | | |
| A1409-65 | 2.10 | 5.2 ±0.5 | 2.5±0.3 | 0.63 | g |
| IC4444 | 0.12 | < 0.5 | < 4.0 | | |
| NGC5643 | 0.30 | 2.1 ±0.5 | 7.0±2.0 | | b |
| NGC6215 | 0.10 | 0.8 ±0.5 | 8.0±5.0 | | |
| NGC6221 | 0.38 | 1.4 ±0.25 | 3.7±0.7 | 0.29 | |
| NGC6240 | 0.31 | 15.4 ±0.8 | 49.5±2.6 | | b |
| NGC6300 | 0.15 | 1.0 ±0.5 | 7.0±3.5 | | |
| Tol1924 | – | < 0.35 | – | | |
| NGC6810 | 0.41 | 0.8 ±0.8 | 2.0±2.0 | | |
| NGC7552 | 0.49 | 2.9 ±0.2 | 5.4±0.7 | 0.92 | b |

Notes: [a] Internal error: $\leq 0.01$ $10^{-17}$ W cm$^{-2}$ $\mu$m$^{-1}$; [b] Line resolved; integrated value given; [c] Position in spiral arm/HII ring north of nucleus; [d] Pk 248+8.1: cf. Baas et al. (1994); [e] cf. Koornneef (1993); [f] Cen A: cf. Israel et al. (1990); [g] Circinus galaxy; [h] from Giuricin et al. (1994): $C \approx$ (ground-based [small beam] 10 $\mu$m flux)–(IRAS 12 $\mu$m flux).

further secure the excitation mechanism. We considered this to be of interest in view of the suggestions by Puxley et al. (1988) and Mouri (1992) that the nuclei of several mildly active galaxies contain radiatively excited $H_2$, rather than the more commonly assumed shock-excited $H_2$. Finally, we measured the extent of excited $H_2$ in the nuclei of half a dozen galaxies[5]. The discussion then centers on a correlation of these new data with information from other spectral regimes.

## 2. Observations

The near-infrared spectroscopy presented here was obtained during several observing runs in the period January 1988 to May 1991. We used the cooled infrared grating spectrometer (IRSPEC) on the 3.6 m telescope at the European Southern Observatory. As the interpretation of the data requires an understanding of the instrumental characteristics, we describe those in some detail.

IRSPEC in the version predominantly used, featured a 32 element array with a pixel spacing of $\lambda/\Delta\lambda \cong 1600$ at 2.2 $\mu$m. The actual resolution of the spectrograph is somewhat better than that, so that lines narrower than a few hundred km s$^{-1}$ are slightly undersampled. We found the sensitivity of the instrument to be very stable within an observing period, but measured variations from run to run of several tens of per cent. Typically, narrow emission features with a line flux of $1.0 \times 10^{-21}$ W cm$^{-2}$ could be measured with an accuracy of about 20% in one hour of elapsed observing time. All observations were chopped in a north-south direction with chopper throws of 20 to 30 arcsec. Data analysis showed that significant spectral structure can occur in the 'zero-flux' baselines even for observations in spectral regions generally considered 'clear', such as the H and K atmospheric windows. As the penalty in observing time is minimal, we included beam-switching in addition to chopping in our routine observing strategy.

Wavelength calibration was done by obtaining spectra of a built-in neon lamp. Repeated observations show that the standard dispersion curves and procedures can provide velocities accurate to about 40 km s$^{-1}$ for sufficiently strong lines. For such an accuracy, it is advisable to obtain the neon spectra with the telescope at the actual source position.We did not always adopt this practice, as accurate radial velocities were not our highest priority. Nevertheless, most of our velocities are good to about 80 km s$^{-1}$.

For flux calibration we used the standard stars HR 191, HR 2290, HR 4523 and HR 6072. We did not observe all standards at all grating settings, but found that HR 191 has significant hydrogen absorption H11-4 at 1.681 $\mu$m for which we corrected; we also see some H7-4 absorption at 2.166 $\mu$m in HR 2290. Otherwise, the flux distributions of our calibrators appear well represented by simple polynomials (Koornneef, 1983a,b).

To convert flux to surface brightness we use the nominal physical size of the entrance aperture ($6 \times 6$ arcsec, or 0.846 nsr). Within the aperture, we found instrumental response to a point source quite sensitive to proper centering even during periods of excellent seeing. Consequently, the point-source based flux calibration leads to an underestimate of the surface brightness for those sources that fill the aperture in a more uniform manner.

Data analysis is relatively straightforward. The first step is to discard data affected by cosmic ray hits (spikes). On science targets, we collected chopped observations on a single position for about 15 minutes. For such a dataset, we separated the readouts for the two chopper positions and remove the datapoints that were statistically out of range. While only a third to half of the (15 minute) spectra have one or more cosmic ray hits, their effect on the spectra is quite disastrous as their appearance closely mimics that of unresolved emission lines. We consider their removal essential for reliable work at the intensity levels considered here. After despiking, positive and negative beams are combined in the usual manner. We then applied a (spectral) vignetting function to compensate for some instrumental curva-

[5]We have generally assumed galaxy distances derived from their radial velocities, corrected for solar motion, and a Hubble constant of $H_0 = 75$ km s$^{-1}$ Mpc$^{-1}$.

ture of the spectrum. The apparent light loss amounts to 10 to 20% at the extreme ends of each spectrum and is calibrated through our observations of the standard stars. The actual spectral vignetting appears to be much less for spatially extended sources, which therefore tend to be overcorrected. Thus, turn-up of the calibrated spectra at the ends of the wavelength band signals that the source is spatially extended.

Extinction coefficients and count-to-flux conversions are applied to each pixel individually. We did not independently determine the grey component of the atmospheric extinction, but adopted typical values from infrared filter photometry instead (e.g., Israel & Koornneef, 1988). Extinction was assumed to depend linearly on airmass, which is adequate for the limited airmass range of our dataset, except for some very narrow and deep absorption lines at 2.418 $\mu$m which left significant residuals. We also found indications that these atmospheric lines vary in strength even during stable weather, presumably due to changes in the precipitable water vapour content of the higher atmosphere.

The repeated readouts within one dataset allow the derivation of an internal error for that particular pointing. We carry this error through the process of beam-combining, devignetting, atmospheric correction and flux calibration. The above process was repeated for each of the approximately 250 spectral scans obtained to support the present paper. Each of the scans covers approximately 7000 km s$^{-1}$ around the individual emission lines (which typically only cover one to two out of the 32 pixels). Apart from the narrow – securely identified – emission lines, none of the scans shows evidence for 'broad' emission structure. Line and continuum fluxes, as well as their ($2\sigma$) errors, were simultaneously obtained by fitting an appropriate multi-parameter function on the whole – 32 pixel – spectrum. The error values associated with the individual pixels in each of the spectral scans were used as weights, and our fitting algorithm assigned the corresponding uncertainties to the output parameters. For the great majority of sources, we obtained multiple scans for each wavelength setting. An analysis of the repeatability provided results consistent with the errors derived from the fitting process. We are thus very confident that the errors associated with our line and continuum fluxes (Tables 1 and 3) provide a proper representation of the internal errors of our measurements. Systematic errors will be discussed in more detail in the text, where appropriate.

We note that the errors 'automatically' associated with the line fluxes are not very sensitively dependent on the fluxes themselves. Apparently, it is only at the very lowest flux levels that the detector/background noise dominates over competing effects such as variations in the seeing/absorption/emissivity of the sky, and incompletely cancelled pixel to pixel (sensitivity) variations.

We refer to our earlier paper on Magellanic HII regions (Israel & Koornneef, 1991) for examples of IRSPEC spectra taken with the same instrumentation and similar signal to noise.

## 3. Results

### *3.1. Comparison with other investigations*

Line fluxes for several $H_2$ transitions, as well as continuum measurements, are summarized in Tables 1 and 3. Within the observed spectral ranges, we also obtained some detections of the HeI $4^3S - 3^3P^0$ and $4^1S - 3^1P^0$ lines, as well as an unidentified feature at 2.1035 $\mu$m. These results will be discussed elsewhere.

We have compared our 1–0 S(1) $H_2$ line fluxes with those quoted by Kawara et al. (1987) (hereafter KNG) and Moorwood & Oliva (1988, 1990) (hereafter MO88, MO90). The result is shown graphically in Fig. 1 (also see Table 2). The agreement with the KNG results (marked by open circles) is satisfactory, with the differences in the flux determinations largely due to their larger aperture size ($9 \times 18$ arcsec as compared to our $6 \times 6$ arcsec.) We will take advantage of the fact that some of these measurements lie systematically above ours to estimate how the $H_2$ emission extends beyond our aperture. We will return to this point later.

The measurements by Moorwood & Oliva were obtained with the same instrument, and should

Table 2
Comparison of 1–0 S(1) fluxes

| Galaxy | 1–0 S(1) Line Flux ($10^{-21}$ W cm$^{-2}$) | | | | |
|---|---|---|---|---|---|
| | KI[a] | MO88[b] | MO90[c] | KNG[d] | Adopted |
| NGC253 | 6.9±0.4 | 11.1±0.5 | 10.8±0.7 | – | 8.5±0.3 |
| NGC1365 | 0.8±0.25 | 2.0±0.6 | – | 1.7±0.3 | 1.5±0.2 |
| NGC1808 [h] | 2.6±0.6 | 4.1±0.7 | – | 2.1±0.4: | 3 ±0.5 |
| NGC1808 [e] | 11.2±1.1 | – | 14 ±1.4 | – | 12 ±0.8 |
| He2-10 | 1.2±0.25 | 1.4±0.3 | – | 0.9±0.2 | 1.2±0.2 |
| NGC2992 | 1.2±0.5 | – | 3.2±1.0 | 1.1±0.7[f] | 1.4±0.4 |
| NGC3256 | 3.8±0.4 | 2.8±0.2 | 4.3±0.8 | 5.7±0.8[f] | 4.0±0.4 |
| NGC4945 | 12.9±0.5 | 10.3±1.0 | 11.9±0.8 | – | 12.5±0.4 |
| A1409-65[g] | 5.2±0.5 | 7.0±1.0 | 9.9±1.8 | 10.1±1.2[f] | 7.0±0.3 |
| NGC6221 | 1.4±0.25 | 3.3±0.8 | 3.4±0.7 | 0.6±0.8[f] | 1.9±0.3 |
| NGC7552 | 2.9±0.2 | 2.9±0.6 | 3.9±0.5 | 3.1±0.3 | 3.1±0.2 |

Notes: [a] This paper: errors shown are about $2\sigma$; aperture $6\times6$ arcsec; [b] Moorwood & Oliva (1988); aperture $6\times6$ arcsec; [c] Moorwood & Oliva (1990); aperture $6\times6$ arcsec; [d] Kawara et al. (1987): apertures $6\times3.8$ and $6\times3$ arcsec unless otherwise indicated; [e] Moorwood & Oliva (1990) (their Table 1) data summed over five positions; our data are summed over four positions; Krabbe et al. (1994) observe $1.1\times10^{-20}$ within a circular 24 arcsec diameter aperture; [f] aperture $9\times18$ arcsec; [g] Oliva et al. (1994) adopt a value of $7.9\times10^{-21}$; [h]Krabbe et al. (1994) observe $3\times10^{-21}$ integrated over a $6\times6$ arcsec aperture.

therefore yield results identical to ours. However, Fig. 1b shows some significant differences in the respective emission line intensities. At least part of this scatter may be due to strongly peaked $H_2$ distributions, which can result in significantly lower fluxes from small pointing and tracking errors. As the line and continuum fluxes typically have similar spatial distributions (see Section 3.4), we investigated the discrepancies by comparing the 2.1 $\mu$m continuum flux levels from our Table 1 with the seven galaxies in common from Figs. 1a and 1b of MO90. For the center of NGC 1808, MO90 provide a spectrum summed over five different positions, and for this galaxy center we took the line and continuum levels from Fig. 1 of Moorwood & Oliva (1989), which can be directly compared to our single pointing. We find the average of the ratio of the MO90 fluxes over ours is 1.08 with a standard deviation of 0.12. This is very encouraging, given the complexity of the observational procedures. We then compared

Table 3
Hydrogen line fluxes of southern galaxy nuclei

| Transition | Line flux ($10^{-21}$ W cm$^{-2}$) | | | | | |
|---|---|---|---|---|---|---|
| | NGC 253 | NGC1808 | NGC3256 | NGC4945 | A1409-65 | NGC6240 |
| 1–0 S(1) | 6.9±0.4 | 2.6±0.6 | 3.8±0.4 | 12.9±0.5 | 5.2±0.5 | 15.4±0.8 |
| 1–0 S(0) | 1.7±0.4 | <0.4 | 0.6±0.2 | 4.4±0.5 | 1.8±0.4 | 3.2±0.9 |
| 2–1 S(1) | 0.9±0.4 | 1.2±0.5 | 0.8±0.2 | 2.3±0.3 | <0.6 | 3.5±0.6 |
| 2–1 S(2) | – | – | – | 0.6±0.4 | – | 0.7±0.6 |
| 2–1 S(3) | – | – | – | – | – | 1.8±0.7 |
| 3–2 S(1) | – | 2.2±1.0 | – | – | <0.4 | – |
| 3–2 S(5) | – | – | – | – | – | 1.3±0.8 |
| 1–0 Q(1) | 8.6±0.3 | 4.9±1.2 | 2.5±0.7 | 14.8±0.7 | 6.3±0.7 | – |
| 1–0 Q(2) | 2.2±0.7 | – | – | 5.1±0.8 | – | – |
| 1–0 Q(3) | 5.3±0.3 | 3.7±1.2: | – | 13.6±0.7 | 2.7±0.8 | – |
| 1–0 Q(4) | 0.5±0.3 | – | – | 2.2±0.8 | – | – |
| Br$\gamma$ | – | – | – | 5.7±0.5 | – | – |

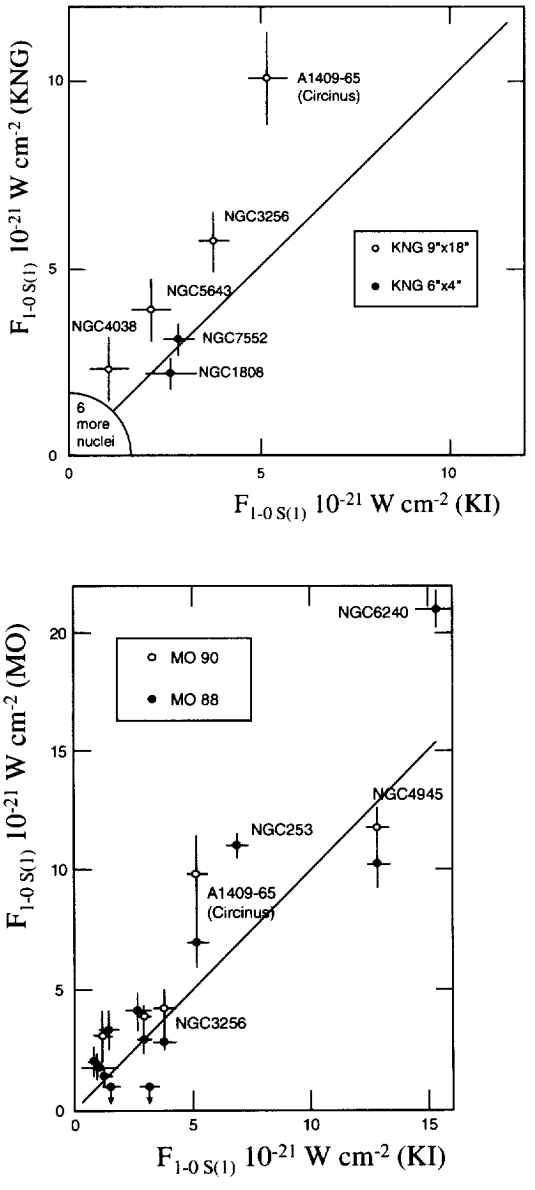


Fig. 1. (a) Comparison between the current $H_2$ 2.121 $\mu$m 1–0 S(1) line fluxes (KI) and those of Kawara et al. (1987) (KNG). The relatively modest increase in observed line fluxes for the larger aperture size shows that the spatial distribution of excited $H_2$ peaks at the nucleus. (b) Comparison between the current data and those of Moorwood & Oliva (1988, 1990) (MO88 & MO90). For a discussion, see Section 3.1.

for these eight galaxies the 1–0 S(1) line strength, normalized to the underlying continuum. This results in an improvement of the correlation between the two sets of line fluxes, which is consistent with the discrepancy in the respective continuum levels being due to differences in calibration and small pointing differences[6]. For five galaxies (NGC 253, 1808, 3256, 4945 and 7552) the normalized fluxes are in excellent agreement, with only a slight tendency for the MO90 fluxes to be higher. But for A1409-65 (the Circinus galaxy), MO90 find a line strength 1.7 times higher, whereas our cross-mapping provides no indication for a significant pointing error. Also, our continuum flux value is within a few percent of the A1409-65 spectrum shown in Fig. 1b of MO90. For NGC 2992 and NGC 6221, MO90 report line fluxes which are at least twice as high as ours. While for any individual galaxy the discrepancy is within the combined uncertainties (note that MO90 tabulate $1\sigma$ errors whereas our errors are about $2\sigma$ as well as smaller in absolute value), we find that the excess of the line fluxes found by MO90 over our values is systematically larger for the fainter lines. Our data analysis procedures include automated profile fitting. With a baseline of 32 pixels and just resolved line features, this procedure was found to work consistently and repeatably, and we know of no obvious mechanism that could cause our line fluxes to be systematically too faint at the lower flux levels. On the other hand, Figs. 1a and b of MO90 show the three most discrepant galaxies to have poorly defined 1–0 S(1) profile shapes, suggesting that their fluxes may have been overestimated. Also, there are significant differences between the MO88 and MO90 data, the former being generally closer to our values.

Taking the above into account, our experience is that changes in the aperture response function and pointing differences of a few arcsec may occasion-

[6]A special case is that of NGC 6240, which van der Werf et al. (1993) have shown to possess an extended and complex source structure with different continuum and line distributions. In particular relevant in this context is their finding that the $H_2$ emission for this galaxy appears not to be centered on the nucleus. The difficulties of measuring the total $H_2$ flux for the center of this galaxy are most effectively demonstrated in their Table 1.

ally influence observed $H_2$ line fluxes of galaxy centers by as much as fifty per cent. To illustrate this conclusion, Table 2 summarizes the 1–0 S(1) fluxes for those galaxies in common between at least three different authors. The final column in Table 2 gives the flux of the 1–0 S(1) line we adopted as based on the assumed errors given and the adopted aperture. The errors we adopted for our 'final' values are again 'internal', i.e. similar to those in Tables 1 and 3.

### 3.2. Equivalent width of the $H_2$ 1–0 S(1) line

In Fig. 2, we compare the detected nuclear 1–0 S(1) strength with the continuum at the same wavelength, measured simultaneously, and in the same aperture. The range of the 1–0 S(1) equivalent width is about a factor of 50, but most of the systems have $1\ \text{Å} < W_\lambda < 10\ \text{Å}$. In a recent study of *ultra*luminous infrared galaxies, Goldader et al. (1995) report a *similar* range, and no obvious correlation between equivalent width and overall nuclear luminosity. Thus, while the $H_2$ 1–0 S(1) luminosities *and* the 2.1 $\mu$m continuum luminosities do generally (Table 9) scale, their ratio does not. Consequently, one would expect the 1–0 S(1) equivalent width – a distance independent and reddening insensitive parameter – to be diagnostically useful. In pure starburst models, the continuum luminosity represents

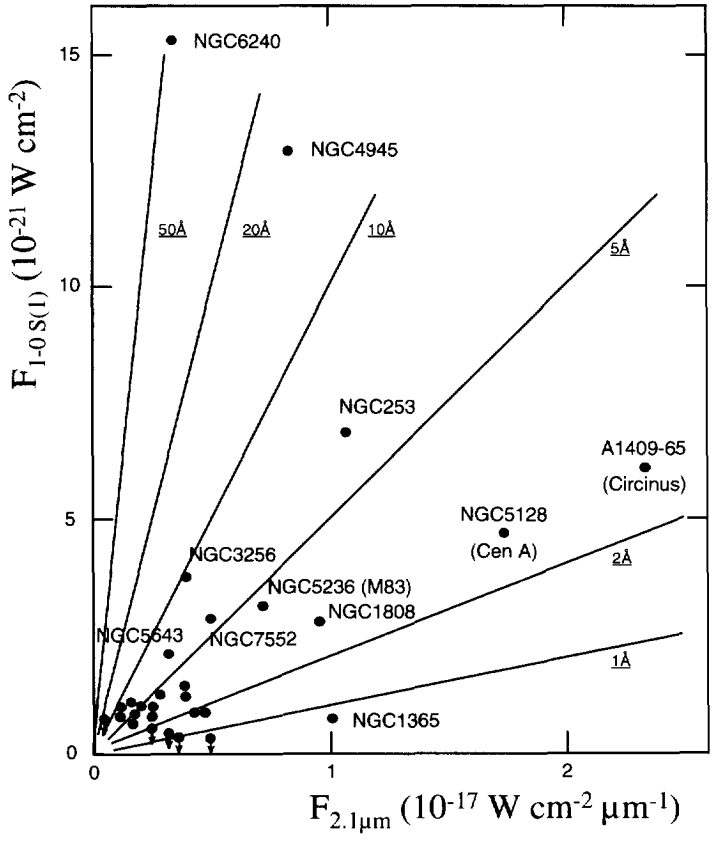


Fig. 2. The relationship between the 2.1 $\mu$m continuum strength and the 1–0 S(1) $H_2$ emission line flux in our sample of galaxy nuclei. Along any of the broken lines, the equivalent width of the emission is constant and has the value shown. In a starburst dominated model, those systems with large equivalent width should generally have high wind powers relative to the total mass of the starburst (e.g., Leitherer et al., 1992). The position of an object in this diagram should thus be sensitively dependent on the evolutionary status of the starburst.

the underlying stellar population, while the $H_2$ emission depends on the mass loss characteristics. The evolution of both these parameters with time and as a function of starburst properties has been modeled (e.g., Leitherer et al. (1992) for young starbursts), but not yet mapped into observables such as the $H_2$ equivalent width. Given the finding that the surface brightness in the 1–0 S(1) line is roughly the same for all systems observed by us (Section 4.4), the *presence* of sufficient amounts of $H_2$ does probably not need to be questioned. The *excitation* of the hot molecular component, which is typically due to shocks (Section 4.2), will change as the wind characteristics of the starburst evolve and the cavity expands (e.g., Suchkov et al., 1994). Note, however, that an expanding cavity exposes a larger surface area to the nucleus, and might well produce more $H_2$ line emission for the same wind energy. Thus, while we would expect the 2.1 $\mu$m luminosity, which is dominated by long living low-mass stars, to evolve more slowly than the mass loss rates (which are dominated by higher mass stars), the $H_2$ 1–0 S(1) equivalent width is not predicted to decrease monotonically with time.

With respect to the currently available diagnostics based on non-thermal radio emission, we note that two (NGC 253 and NGC 4945) out of the galaxies with the highest 1–0 S(1) equivalent widths have compact nuclear radio sources that contribute half or more to the integrated radio emission. This suggests that for these systems the ratio between energy injection by supernovae relative to the stellar winds is relatively high.

### 3.3. Observations of other $H_2$ transitions

In the seven brightest galaxies, we observed several additional $H_2$ transitions in an attempt to obtain information on the excitation mechanism of the molecular hydrogen. These include the 1–0 S(0) and 2–1 S(1) transitions, as well as the 1–0 Q-branch. Some additional transitions were observed in NGC 6240, as well as NGC 1808 and 4945 (cf. Table 3). There is reasonable agreement with the 1–0 S(0) and 2–1 S(1) values tabulated by MO90 for four of the five galaxies in common (NGC 253,

Table 4
Hydrogen line ratios in southern galaxy nuclei

| Transition | Line Flux/Line Flux$_{1-0\,S(1)}$ | | | | | | |
|---|---|---|---|---|---|---|---|
| | NGC 253 | NGC1808 | NGC3256 | NGC4945 | NGC5128 | A1409-65 | NGC6240 |
| 1–0 S(1) | ≡ 1.00 | ≡ 1.00 | ≡ 1.00 | ≡ 1.00 | ≡ 1.00 | ≡ 1.00 | ≡ 1.00 |
| 1–0 S(0) | 0.25±0.06 | < 0.20 | 0.16±0.05 | 0.20±0.03[a] | 0.48±0.17 | 0.35±0.05 | 0.21±0.06 |
| 2–1 S(1) | 0.13±0.06 | 0.46±0.20 | 0.21±0.05 | 0.18±0.03 | < 0.31 | < 0.12 | 0.23±0.04 |
| 2–1 S(2) | – | – | – | 0.05±0.03 | < 0.24 | – | 0.05±0.03 |
| 2–1 S(3) | – | – | – | – | – | – | 0.12±0.05 |
| 3–2 S(1) | – | 0.85±0.40 | – | – | – | < 0.08 | – |
| 3–2 S(5) | – | – | – | – | – | – | 0.08±0.05 |
| 1–0 Q(1) | 1.25±0.07 | 1.89±0.46 | 0.66±0.18 | 1.15±0.05 | 0.86±0.22 | 1.21±0.10 | – |
| 1–0 Q(2) | 0.32±0.11 | – | – | 0.40±0.06 | < 0.19 | – | – |
| 1–0 Q(3) | 0.77±0.07 | 1.42±0.46: | – | 1.07±0.05 | 0.86±0.22 | 0.52±0.10 | – |
| 1–0 Q(4) | 0.07±0.04 | – | – | 0.17±0.06 | < 0.19 | – | – |
| Brγ | 4.5 [b] | 1.3 [f] | 1.4 [e] | 0.49±0.04[a] | < 0.29 | 0.48 [d] | 0.022 [c] |

Notes: All ratios are derived from the present data, except where indicated:
[a] Koornneef (1993); [c] van der Werf et al. (1993); [e] Kotilainen et al. (1995);
[b] Prada et al. (1996); [d] Oliva et al. (1994); [f] Krabbe et al. (1994).

Table 5
Mean observed and model hydrogen line ratios

| Transition | Line Flux/Line Flux$_{1-0S(1)}$ | | | | | | | | | |
|---|---|---|---|---|---|---|---|---|---|---|
| | (2) SD2A | (3) SD2B | (4) SD2C | (5) SD2D | (6) #14 | (7) S1 | (8) S2 | (9) SH3.3 | Mean: observed | Mean: extinction corrected |
| 1–0 S(1) | ≡1.00 | ≡1.00 | ≡1.00 | ≡1.00 | ≡1.00 | ≡1.00 | ≡1.00 | ≡1.00 | ≡1.00 | ≡1.00 |
| 1–0 S(0) | 0.48 | – | 0.34 | 0.27 | 0.46 | 0.27 | 0.21 | 0.2–0.3 | 0.28±0.06 | 0.26±0.04 |
| 2–1 S(1) | 0.56 | 0.75 | – | 0.02 | 0.56 | 0.01 | 0.08 | 0.0–0.2 | 0.22±0.06 | 0.19±0.04 |
| 2–1 S(2) | 0.32 | – | – | – | 0.28 | 0.00 | 0.03 | 0.0–0.1 | 0.05: | 0.05: |
| 2–1 S(3) | 0.38 | – | – | 0.02 | 0.35 | 0.00 | 0.08 | 0.0–0.3 | 0.12: | 0.12: |
| 1–0 Q(1) | 0.86 | – | 0.85 | 1.12 | 0.99 | 1.05 | 0.70 | 0.5–1.1 | 1.17±0.19 | 0.90±0.10 |
| 1–0 Q(2) | 0.53 | – | 0.38 | 0.30 | 0.51 | 0.30 | 0.23 | 0.2–0.3 | 0.30±0.10 | 0.24±0.05 |
| 1–0 Q(3) | ≡0.70 | ≡0.70 | ≡0.70 | ≡0.70 | ≡0.70 | ≡0.70 | ≡0.70 | ≡0.70 | 0.93±0.17 | ≡0.70 |
| 1–0 Q(4) | 0.34 | – | 0.09 | 0.16 | 0.28 | 0.15 | 0.21 | – | 0.12±0.06 | 0.09±0.05 |

Notes: Column 2: UV-irradiated, $n = 10^3$ cm$^{-3}$; Sternberg & Dalgarno (1989), Table 2A; Column 3: UV-irradiated, $n = 10^4$ cm$^{-3}$; Sternberg & Dalgarno (1989), Table 2B; Column 4: UV-irradiated, $n = 10^5$ cm$^{-3}$; Sternberg & Dalgarno (1989), Table 2C; Column 5: UV-irradiated, $n = 10^6$ cm$^{-3}$; Sternberg & Dalgarno (1989), Table 2D; Column 6: UV-irradiated, $n = 10^3$ cm$^{-3}$; Black & van Dishoeck (1987), Table 2; Column 7: Thermal emission from shock, 1000 K; Black & van Dishoeck (1987), Table 2; Column 8: Thermal emission from shock, 2000 K; Black & van Dishoeck (1987), Table 2; Column 9: J-type shock 6–14 km s$^{-1}$, $n = 3 \times 10^5$ cm$^{-3}$; Shull & Hollenbach (1978), Table 3, block 3.

3256, 4945 and A1409-65), bearing in mind the discussion in Section 3.1. The agreement for NGC 1808 is poor. When we consider the line *ratios* given in Table 4, the agreement is very satisfactory, except again for NGC 1808[7]. The tabulated S transitions are generally considerably (on average four times) weaker than the principal 1–0 S(1) line. The 1–0 Q(3) line is of a strength similar to the 1–0 S(1) line, or slightly weaker, whereas the 1–0 Q(1) line tends to be somewhat stronger than the 1–0 S(1) line.

### 3.4. Extent of $H_2$ emission in galaxy centers

The presently available data allow us to estimate the extent of central $H_2$ emission, and compare it to the extent of stellar 2.1 $\mu$m emission. We previously published a 7 point map of NGC 5128 (Cen A, Israel et al. (1990), while we here (Fig. 3) present a small map (15 points spaced 5 arcsec) of NGC 4945. In both NGC 3256 and A1409-65 we measured emission along, and perpendicular to, the major axis with 3 arcsec spacing down to at least the half-power points. Finally, we observed a few positions along the major axis of NGC 1808, 6221 (3 arcsec separation) and 7552 (4.5 arcsec separation). The results for these last three galaxies are therefore less accurate than for the other four. Numerical results are given in Table 6. The mean extent of $H_2$ emission can also be roughly estimated from comparison of line strengths observed in different apertures. To this end, we compared the strengths observed at La Silla (this paper; MO88 and MO90) with those observed by KNG in a $9 \times 18$ arcsec aperture and by Puxley et al. (1988) (hereafter PHM) in a circular 19.6 arcsec aperture. These estimates are also given in Table 6. For five galaxies, $H_2$ extent determined by offset pointing could be compared to extent estimated from aperture comparison. The

[7]These discrepancies are possibly related to the source structure of NGC 1808, which includes circumnuclear emission on a scale of approximately 15″ (Dahlem et al., 1994; Krabbe et al., 1994), i.e. exceeding the size of our aperture. Note that Krabbe et al. define the K-band luminosity as 'the total luminosity in the 1.9 to 2.5 $\mu$m K-band for a frequency independent K-band flux density'. This results in $\log L_K/L_\odot = (-M_K - 0.38)/2.5$, with the consequence that $L_K$(Krabbe et al.)/$L_{2.2\,\mu m}$(Devereux 1989) = 0.031.

Table 6
Half-intensity sizes[a] of galaxy centers

| Galaxy | $D$ | 2.1 $\mu$m continuum | | 1–0 S(1) $H_2$ | | | Note |
|---|---|---|---|---|---|---|---|
| | | $\alpha$ | $2R$ | $\alpha$ | $2R$ | $\sigma$ | |
| | Mpc | arcsec | kpc | arcsec | kpc | $10^{-5}$ erg s$^{-1}$ cm$^{-2}$ ster$^{-1}$ | |
| NGC 253 | 2.5 | – | – | 9 × 3 | 0.11 × 0.04 | 24 | b,k |
| NGC1068 | 18 | – | – | 2 × 2 | 0.17 × 0.17 | | c |
| | 18 | – | – | 7 × 4 | 0.6 × 0.35 | 15 | d |
| NGC1365 | 21 | – | – | 12 | 1.0 | 7 | e |
| NGC1808 | 11 | 9: | 0.45: | 9(15 × 5) | 0.45(0.8 × 0.3) | 3 | f |
| NGC2992 | 28 | – | – | 3(9 × 1) | 0.4 (1.2 × 0.2) | 11 | g |
| NGC3079 | 16 | 4 × 2 | 0.3 × 0.15 | 4 × 2 | 0.3 × 0.15 | 75 | h |
| NGC3256 | 37 | 6 × 6 | 1.1 × 1.1 | 6 × 6 | 1.1 × 1.1 | 12 | |
| NGC4945 | 6.7 | 7 × 4 | 0.22 × 0.13 | 7 × 7 | 0.22 × 0.22 | 33 | |
| NGC5128 | 3 | 10 × 5 | 0.2 × 0.1 | 4 | 0.06 | 23 | l |
| NGC5236 | 3.7 | – | – | 4.5 | 0.08 | 13 | f |
| NGC5253 | 3.5 | – | – | 3 | 0.05 | 11 | g |
| A1409-65 | 4 | 9 × 5 | 0.2 × 0.1 | 17 × 3 | 0.33 × 0.06 | 24 | |
| NGC5643 | 16 | – | – | 6 | 0.45 | 6 | g |
| NGC6221 | 20 | 5 | 0.5 | 7 | 0.65 | 5 | i |
| NGC6240 | 100 | – | – | 2.3 × 1.7 | 1.1 × 0.8 | 374 | g |
| NGC6300 | 15 | – | – | 5: | 0.35: | 4 | g |
| NGC7552 | 20 | 5 | 0.5 | 7 | 0.7 | 8 | i |
| mean value | – | – | 0.45±0.13 | – | 0.43±0.09 | 17±5 | j |

Notes: [a] aperture size (5″ for PA = 0°; 7.4″ for PA = 45°, etc.) subtracted in quadrature; [b] cavity diameter from Carlstrom et al. (1990); [c] from Rotaciuc et al. (1991); FWHM value given; [d] from Rotaciuc et al. (1991); FW value given; [e] based on comparison of IK and PHM aperture comparison only; [f] based on limited mapping and comparison of IK and PHM aperture comparison; [g] based on comparison of IK and large KNG aperture only; [h] unpublished observations; [i] based on limited offset pointings and comparison of IK and large KNG aperture; [j] surface brightness average: not including NGC6240; [k] the FWHM along the major axis is in good agreement with IRSPEC measurements by Prada et al. (1996); [l] the distance adopted for this galaxy is significantly smaller than would follow from a pure Hubble flow (Frogel et al., 1987; Harris et al., 1984; Hui et al., 1993).

results are in good agreement for all galaxies, with the obvious exception of A1409-65, which our measurements show to extend well beyond the KNG aperture.

In general, the $H_2$ extent is similar to that of the (stellar) continuum at 2.1 $\mu$m. In NGC 4945, the $H_2$ size along the major axis is about the same as the continuum size (Koornneef, 1993). Perpendicular to the major axis, the present study does indicate an $H_2$ FWHM size of about 7″, i.e. similar to the value along the major axis, while the continuum size perpendicular to the major axis is definitely smaller (Koornneef, 1993; Moorwood & Oliva, 1994). For the second case where we have information on the spatial distribution of the excited molecular hydrogen and the near-infrared continuum, i.e. that of A1409-65 (Circinus): again we find (see Table 6) flattened spatial distributions. The $H_2$ size along the major axis of 17″ might possibly be overestimated due to the relatively noisy line data, but our continuum size of 9″ × 5″ is apparently inconsistent with the FWHM size quoted by Moorwood & Origlia (1991) on the basis of subarcsec resolution K-band images. The latter authors argue for both NGC 4945 and A1409-65 that the continuum size of the nucleus changes by about a factor of 3 from 1.25 to 2.2 $\mu$m. This apparent change is very likely the result of strongly non-gaussian light distributions, with the

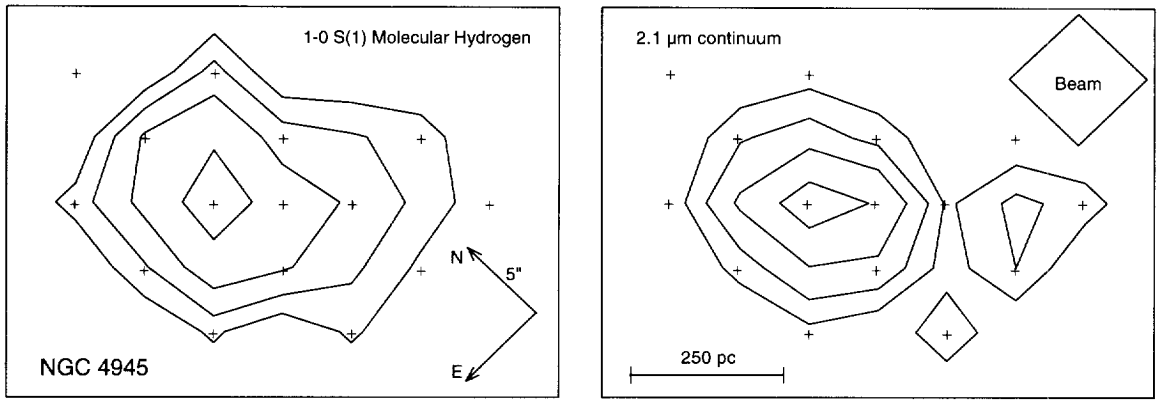


Fig. 3. The spatial distribution of the 1–0 S(1) emission, due to molecular hydrogen, and the 2.1 $\mu$m continuum, as measured by placing the square IRSPEC aperture at several positions around the nucleus of NGC 4945 (as indicated with + signs.) The contours used are at 80, 50, 30, and 15% of the peak intensity – the lowest contour is uncertain due to incomplete sampling. The major axis of NGC 4945 has a position angle of 45°, and runs therefore left to right in this figure. We propose that the observed NE-SW asymmetry of the continuum, the $H_2$ 1–0 S(1) line, and hydrogen Br$\gamma$ (Section 4.2), point towards higher extinction of the nucleus on the NE-side. Note that the extent of the molecular hydrogen emission perpendicular to the major axis exceeds that of the continuum emission, indicative of the presence of a small diffuse component in the outflow in addition to the shocked interface with the circumnuclear ring.

result that the deduced FWHM sizes will become strongly dependent on the placement of the zeroflux level. The high-resolution imaging observations of NGC 1068 by Rotaciuc et al. (1991) show that in that case the full size of the central $H_2$ source is about the same as the FWHM size of the continuum source. Their observations also show significant structure in the $H_2$ distribution of NGC 1068 at scales of about 100 pc. Such structure was also seen in the long-slit spectroscopy of NGC 4945 (Koornneef, 1993), but the spatial resolution of the current data set is generally insufficient for such purposes.

Thus, with some provisos and exceptions (NGC 6240!), the similarity of the spatial distributions of the hydrogen lines and the stellar continuum is rather striking, at least on scales larger than 100 pc.

## 4. Discussion

For two of the galaxies in our dataset, NGC 4945 and A1409-65, we have enough new information on the spatial distribution of the observed near-infrared radiation to justify a separate discussion. Various aspects of the dataset as a whole follow in subsequent sections.

### *4.1. NGC 4945 & A1409-65: two well studied cases*

Our mapping of NGC 4945 reveals that the 1–0 S(1) flux drops by 20% at positions only half an aperture (3 arcsec) away from the peak. The 2.1 $\mu$m continuum, due to nuclear starlight, is also strongly peaked. While the strong peaking of both emissions is the predominant feature, the contour maps of Fig. 3 contain additional information, allowing more detailed conclusions. In particular, we find that the elongated distribution of the 2.1 $\mu$m continuum and the molecular hydrogen line emission is asymmetrical, with the SW side somewhat more prominent. An asymmetry of this type is also noticeable in the position-velocity diagram for Br$\gamma$ (Koornneef (1993); Fig. 2), as well as in the continuum profile in

that same figure[8]. The SW side of the nucleus is the one approaching the observer, implying that the redshifted side is the fainter one. Circular symmetry of the various components in the plane of this galaxy can therefore not be an appropriate assumption on radial distance scales in excess of 200 pc. We propose that the molecular annulus between 200 and 500 pc (see Bergman et al., 1992) contains more dust on the NE side of the nucleus than on the SW side. One possibility is that we are seeing the effects of a bar in the spiral system of NGC 4945, a suggestion first made by de Vaucouleurs (1964). However, Agüero & Carranza (1986) emphasize the difficulties of assessing the morphology of NGC 4945, and argue that this galaxy is unlikely to have a barred spiral. In general, the existence of a bar in late-type spirals has been shown observationally to be well correlated with nuclear activity and high IRAS fluxes, and provides an attractive mechanism for fueling a massive nucleus (e.g., Norman, 1991; Kennicutt, 1994; Knapen et al., 1995). We can therefore not resist rekindling the possibility of seeing (the remnant of) a bar in NGC 4945.

As also follows from Fig. 3, the 2.1 $\mu$m continuum size for the core of NGC 4945 is compatible with the nuclear 6 GHz radio continuum size of $5.7\pm0.1 \times 2.0\pm0.1$ arcsec ($180 \times 65$ pc), where the larger of the two dimensions is aligned with the major axis of the galaxy (Whiteoak & Wilson, 1990). In this comparison, we emphasize the 50% contour, as at lower intensity levels a contribution from the disk, which is projected on the nucleus due to the large inclination of the galaxy (inclination $i = 78°\pm2°$, Ables et al. (1987)) becomes likely. We previously identified the compact radio source with an evolved starburst cluster with $M_{\rm stars} \leq 1.2\pm0.4 \times 10^9\ M_\odot$ (Koornneef, 1993). While we did not spatially resolve the 2.1 $\mu$m continuum emission perpendicular to the major axis with the limited resolution available with the square aperture version of IRSPEC, the molecular hydrogen emission *is* spatially resolved in this direction (also see Table 6). Dynamically, the molecular material is gravitationally bound to the starburst nucleus, with most orbits within a thick disk, or torus. Most of the $H_2$ emission comes from a region comparable to the inner radius of the molecular ring, with an additional contribution from a diffuse component. Excitation of the molecular hydrogen results from the strong outflow from the nucleus, which itself is a combination of SNRs and mass loss from red supergiants. The relative contributions of these two components, in mass, chemical composition, momentum and energy, are not well known. Interestingly, Moorwood & Oliva (1994) have shown that the spatial distribution of the 1.64 $\mu$m [FeII] emission line is very similar to that of the excited molecular hydrogen. This raises the distinct possibility that, in NGC 4945, a significant fraction of the [FeII] emission is also circum*nuclear* (with a characteristic scale size of 200 pc; Koornneef, 1993). This is in contrast with the canonical explanation, which attributes the [FeII] emission in galactic nuclei to (a superposition of) compact SN remnants, i.e. to the circum*stellar* regime. The observation that the [FeII] emission is more extended than the 2.1 $\mu$m near-infrared and the 6 GHz radio continuum, which should delineate the spatial distribution of the starburst and the SN progenitors respectively, presents an interesting challenge. One consideration is that the physics of the intracluster medium in a starburst does differ significantly from that of the interstellar medium usually considered in the study of (Galactic) SNe and their remnants. For example, in a starburst system like NGC 4945, with a stellar density of about $10^3\ M_\odot\ {\rm pc}^{-3}$, and a mass flux with ram pressure $p \equiv n_0 v_s^2$ of $7.7 \times 10^7\ {\rm cm}^{-3}\,({\rm km\,s}^{-1})^2$ (Koornneef, 1993) the formation of [FeII] emitting regions around newly exploded stars could well be inhibited[9]. Instead, a

[8]Nuclear near-infrared images of NGC 4945 were recently obtained with a tunable imaging Fabry-Pérot (Moorwood et al., 1996). These images generally compare favourably with our results, except that their Br$\gamma$ image shows an asymmetry in favour of the NE side, which we do not confirm.

[9]Likewise, the usage of stellar evolution models developed for field stars might well be quite inappropriate for describing the evolution of stars in a massive starburst.

significant fraction of the observed [FeII] emission apparently occurs in the high density gas associated with the same fast circumnuclear shock that it also responsible for the excitation of $H_2$, as well as the ionization of some HI. The possibility that, in NGC 253, "the [FeII] emitting region is not located close to the nucleus but may be associated with gas shockexcited by the superwind" was earlier raised by MO88. Under these circumstances, it is not clear that the [FeII] 1.64 $\mu$m luminosity provides a reliable method for estimating the SN rate, as has been argued (e.g., Forbes, 1993). We also refer to near-infrared (AAT–IRIS) images in the $H_2$ and [FeII] lines of the northern section of the Orion nebula (Allen & Burton, 1993). The distribution suggests the presence of wakes left behind by objects violently blown out; the wakes are lit up by low-energy shocks. At the tips of these wakes, 'shrapnel' from the explosion is seen emitting [FeII] line radiation, excited by high-energy shocks.

The multiple pointings for A1409-65 yield results for the spatial distribution of the $H_2$, and continuum distributions which differ in detail from those derived for NGC 4945. In particular, we find that the $H_2$ emission, as measured along the major axis, has only dropped to about half 9 arcsec (NE and SW) from the nucleus, while in the direction perpendicular to the major axis, we see 20% of the peak value only 6 arcsec (NW and SE) from the maximum. The drop of the continuum fluxes is closely similar between these two directions. In other words, while the peak equivalent width for A1409-65 is about 2.5 Å, it increases to about 5 Å about 9 arcsec away from the nucleus in the direction of the major axis, and drops to about 1 Å 6 arcsec perpendicular to the major axis. The corresponding entries for A1409-65 in Table 6 reflect this difference. Oliva et al. (1994) studied the Seyfert 2 nuclear component of this galaxy and found a very compact coronal line region, free of dust and photoionized by the nucleus. In particular their [NII] observations (cf., their Fig. 4) suggest the presence of an additional component in the form of a rotating torus with a radius of approximately 10″.

### *4.2. Extinction and excitation of $H_2$ in galaxy centers*

The directly observed extragalactic line ratios, given in Table 4 (see Section 3.3) already suggest that, within the errors, the observed $H_2$ is largely or completely shock-excited. This is illustrated in Fig. 4, where we have plotted the observed line strength ratios of 1–0 S(0)[10], respectively 2–1 S(1) versus 1–0 S(1) emission. In addition, we have plotted the same ratios of a number of (mostly fluorescently excited) extragalactic HII regions taken from Israel & Koornneef (1991), as well as model ratios for fluorescent excitation and thermal (shock) excitation assuming different temperatures (cf. Israel & Koornneef (1991); MO90). The galaxy points all cluster near the line of thermal excitation; but systematically displaced in the direction of the fluorescent line ratios. This displacement is at least partly due to differential reddening between the wavelengths of the relevant transitions (see Section 4.2), but a small contribution ($< 25\%$) by fluorescently excited emission cannot be excluded. However, *most of the emission must originate from shock-excited* $H_2$. After allowance for differential extinction and/or a possible fluorescent component, the mean thermal excitation temperature is close to 2000 K (e.g., Brand et al., 1989; Mouri, 1994). As our observed value for the 2–1 S(1)/1–0 S(1) ratio for the nuclear region of NGC 3256 is significantly below the value reported by Doyon et al. (1994), we do not confirm their conclusion that UV fluorescence in that galaxy is responsible for at least 60% of the 1–0 S(1) emission. Of course, at very high densities ($n_H = 10^5$–$10^6$ cm$^{-3}$), fluorescent emission line ratios can mimic thermal excitation (Sternberg & Dalgarno, 1989) but we have no observational indications that

[10]Depending on the radial velocity of the galactic nucleus, the accuracy of the 1–0 S(0) data can be limited by the presence of two fairly strong terrestrial atmospheric emission lines due to vibrationally excited OH at 2.2245 & 2.2311 $\mu$m. The spectral power in these lines can vary by several percent on time scales of a few minutes.

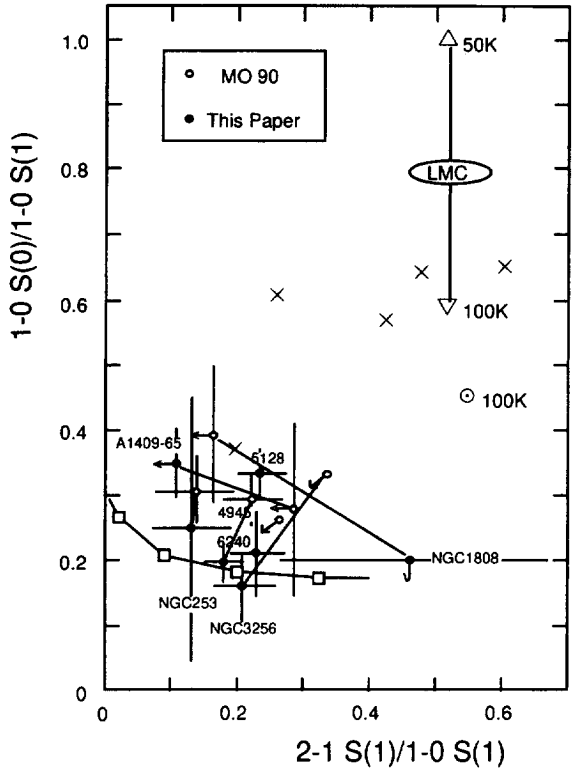


Fig. 4. We show (○ and ● signs) the observed strengths of the 2–1 S(1) and 1–0 S(0) emission lines relative to the 1–0 S(1) line, all due to molecular hydrogen, for various galaxy nuclei. The heavy solid track predicts the line ratios as a function of temperature for purely thermal, i.e. shock-, excitation conditions, with model temperatures of 1000, 2000, 3000 & 4000 K (left to right) marked with □ signs. Models for purely radiative, i.e. fluorescent-, excitation in an environment with solar abundances (Black & van Dishoeck, 1987) at a temperature of 100 K yield the line ratios indicated with the ⊙ sign. The × signs represent observations by Israel & Koornneef (1991) of various extragalactic (LMC, SMC & M33) HII regions, which are predominantly radiatively excited. From that same reference we copied the model track (terminated with △ & ▽ signs) for fluorescent excitation at LMC abundances. Models for fluorescent excitation in very high density regions can be found in Sternberg & Dalgarno (1989), but have not been explicitly shown to avoid confusion (see Section 4.2). Note that some of the galaxy nuclei earlier observed by Moorwood & Oliva (1990) are located significantly closer to the thermal excitation line in our observations.

the unlikely combination of high density *and* a strong ultraviolet radiation field can occur *throughout* the very extended regions where we observe excited molecular hydrogen, and at least in some of the cases we know that there is a paucity of ultraviolet photons.

In principle, one can determine the extinction of the observed $H_2$ emission, by comparing the observed ratio of 1–0 Q(3) to 1–0 S(1), which arise from the same upper level, with the $A$-value ratio of 0.70. (This leads, in magnitudes, to an extinction $A_{2.1\ \mu m} = 12.5\log(1.43F_{Q3}/F_{S1})$; Scoville et al. (1982).) While the observational errors associated with our data are small, the inferred infrared extinction values are quite uncertain as the two $H_2$ transitions are only 0.3 $\mu$m apart in wavelength. Nevertheless, our determinations of the extinction at 2.1 $\mu$m, the wavelength of the 1–0 S(1) transition, suggest that NGC 3256, A1409-65 (Circinus), and possibly NGC 6240 do not suffer significant extinction. For NGC 253 we find $A_{2.1\ \mu m} = 1.0\pm0.5$ mag, for NGC 1808 $A_{2.1\ \mu m} = 3.8(+1.5, -2.1)$ mag and for NGC 4945 2.3±0.3 mag[11]. For NGC 5128 (Cen A) we find, using the data given by Israel et al. (1990), an extinction $A_{2.1\ \mu m} = 1.1\pm1.1$ mag. Dereddening the observed data, with an $A_\lambda \propto \lambda^{-1.7}$ extinction law, results in the 'mean' line ratios given in column 9 of Table 4. Relative to the observed data, the scatter has decreased, and most galaxy points of Fig. 4 would move closer to the thermal (shock) excitation line; while the 'mean' thermal excitation temperature decreases slightly. This behaviour boosts

[11]This value is significantly higher than the value derived by Koornneef (1993) from multi-aperture photometric photometry under the assumption that the non-nuclear contribution to the optical light distribution is spatially uniform over a 34″ diameter region. However, recent images of the nucleus of NGC 4945 with the *Planetary Camera2* (F606W filter) onboard the *Hubble Space Telescope* show a very dark dust lane running across the position of the nucleus. We therefore prefer the current value for the extinction. One consequence is that the absolute magnitude of the nuclear starburst ($M_K$) is higher than we previously assumed, and must be close to the value for M82.

our confidence in the validity of the extinction corrections, at least in a statistical sense. Therefore, the fact that in our, admittedly small, sample the highest extinctions tend to occur in the galaxies with the smallest $H_2$ extent (cf. Table 6) might not be just due to chance.

The potentially large extinctions at 2.1 $\mu$m introduce non-negligible differential reddening between the H and K windows, and even within the K window itself. Thus, relations found between the observed strengths $H_2$, [FeII], Br$\gamma$ and 3.28 $\mu$m emission features (see e.g., MO88, Kawara et al., 1988; Mouri et al., 1990a,b, 1993) are potentially subject to significant revision if differential reddening is included (see also van der Werf et al. (1993) for the case of NGC 6240). As a, rather puzzling, example we mention that in our own sample the observed line ratio $H_2$ 1–0 S(1)/[FeII] for the galaxies appears to increase linearly with the observed $H_2$ extent. However, this relation virtually disappears if we introduce our proposed reddening corrections. This might indicate that [FeII] is more centrally concentrated than $H_2$, causing less extinction for [FeII] as compared with $H_2$.

Using total $H_2$ fluxes and sizes obtained from Tables 1,2,5, we have determined the 1–0 S(1) surface brightness of the $H_2$ emitting zones. Apart from having considerable observational uncertainty, the resulting values given in Table 6 are lower limits, as a homogeneously filled emitting surface is assumed and extinction is neglected. If instead the emission arises in a dusty torus, as appears to be the case at least in NGC 1068 (but see Cameron et al., 1993; Neff et al., 1994) and NGC 5128 (cf. Rotaciuc et al., 1991; Israel et al., 1990), the actual surface brightnesses may be considerably higher. The lower limits in Table 6 range from $2.5 \times 10^{-5}$ to $3.2 \times 10^{-4}$ erg s$^{-1}$ cm$^{-2}$ ster$^{-1}$. For comparison we note that such values can occur, according to model calculations for C-type MHD shock waves by Draine et al. (1983), with shock velocities of 20–30 km s$^{-1}$ into a neutral medium with density of order $n_H = 10^4$ cm$^{-3}$, and magnetic fields of approximately 50–100 $\mu$Gauss.

### 4.3. Luminosities of galaxy centers

Based on the single aperture fluxes and the deduced $H_2$ extent[12], we have calculated luminosities emitted in the S(1) line[13] for the galaxies in Table 6, and entered the results in Table 8. $L_{1-0S(1)}$ ranges from about $10^4 L_\odot$ for NGC 5128, NGC 5236, and NGC 5253, about $5 \times 10^5 L_\odot$ for NGC 1808, NGC 2992, NGC 4945, NGC 5643, and NGC 7552, $3 \times 10^6 L_\odot$ for NGC 3256, while NGC 6240 (with $L_{1-0\,S(1)}/L_\odot \approx 8.4 \times 10^7$) is well into the ultraluminous class (ultraluminous infrared galaxies typically have $L_{1-0S(1)}/L_\odot \approx 10^7$, e.g., Goldader et al. (1995).) This implies[14] total mechanical luminosities of the winds impacting the shocked $H_2$ zone ranging from about $10^8$ to several times $10^{10} L_\odot$. For this calculation we did not apply extinction corrections, as these are not known with sufficient accuracy for all of galaxies in the sample. However, we do not expect differences in reddening between individual galaxies to make a great impact, statistically, as we could not determine a solid correlation between extinction and, for example, the extent of the $H_2$ emitting region. From the same data

[12] We emphasize that $L_{1-0S(1)}$ in Table 8 is calculated explicitly by multiplying the observed peak values in Table 1 with the ratio of the deduced 'observed' area to the observing aperture. Therefore, the listed $L_{1-0S(1)}$ values represent in principle *all* the central $H_2$ emission, not just that in our aperture. Also, while – for example – the radio emitting region might be larger still (e.g., in NGC 253 & NGC 2992), comparisons between luminosities remain straightforward as long as the exciting energies predominantly originate in the central region.

[13] Line fluxes (e.g., [FeII], 1–0 S(1) & Br$\gamma$ at 1.64, 2.12 & 2.17 $\mu$m) convert to luminosities in a straightforward manner: $L_{line} = 1.20 \times 10^{29} F_{line} D^2$, with $L_{line}$ in W, if $F_{line}$ is in units of $10^{-21}$ W cm$^{-2}$, and $D$ in Mpc. The result translates into solar luminosity units by dividing through $3.826 \times 10^{26}$.

[14] For low velocity shocks, $L_{1-0S(1)}/L_{wind} \lesssim 0.02$ (Draine et al., 1983), while high velocity shocks are much less efficient (e.g., Hawarden et al. (1995) derive $L_{1-0S(1)}/L_{wind} \simeq 6 \times 10^{-5}$ for NGC 3079).

Table 7
21 cm radio continuum flux densities of galaxy centers

| Galaxy | $S$ (21 cm) (Jy) | Size (arcsec) | Remarks | Reference |
|---|---|---|---|---|
| NGC 253 | 2.6±0.2 | 20 | nucleus | 1,2,3 |
| NGC1068 | 1.7±0.1 | 1 | nucleus | 2 |
| | 3.9±0.2 | 15 | center & jets | 2,3 |
| NGC1365 | 0.45±0.02 | 20 | nucleus | 1,3,5,6 |
| NGC1808 | 0.43 | 18 × 12 | center | 7 |
| NGC2992 | 0.27±0.07 | 35 | center | 8 |
| NGC3079 | 0.16±0.02 | 5 | nucleus | 2 |
| | 0.43p | 15 | center | 3 |
| NGC3256 | 0.62 | < 18 | center | 3 |
| NGC4945 | 4.8 | 12 × 4 | nucleus | 1,9,13 |
| NGC5128 | 0.11 | < 1 | nucleus | 10 |
| | 3.4 | | center & jets | 11 |
| NGC5236 | 0.44 | 45 × 25 | center | 1,3,12 |
| NGC5253 | 0.072 | 24 × 18 | center | 3 |
| A1409-65 | 0.82±0.02 | 23 × 18 | center | 1,9 |
| NGC5643 | 0.035±0.05 | < 36 | center | 3 |
| NGC6221 | 0.19±0.09 | – | center | 5 |
| NGC6240 | 0.23±0.03 | 5 | center | 2 |
| NGC6300 | 0.06±0.03 | – | center | 5 |
| NGC7552 | 0.22 | 30 × 24 | center | 3,8 |

References:
1. Bosma et al. (1983);
2. Condon et al. (1982);
3. Condon (1987);
4. Wynn-Williams et al. (1985);
5. Harnett (1987);
6. Sandquist et al. (1982);
7. Saikia et al. (1990);
8. Ward et al. (1980);
9. Whiteoak & Bunton (1985);
10. Tzioumis (1987);
11. Schreier et al. (1981);
12. Ondrechen (1985);
13. Ables et al. (1987).

we also derived a value for the 2.1 $\mu$m continuum luminosity[15,16].

We may compare these luminosities to monochromatic mid-infrared luminosities $L_{12\,\mu m}$ (derived from IRAS PSC data) or 21 cm monochromatic radio continuum luminosities[17] of the nucleus/central region wherever these are available. The mid-infrared luminosities refer to apertures of order 0.75 × 4.5 arcmin, and thus cover substantially larger surface areas than covered by the extent of $H_2$ emission. Galaxies with a disk more or less completely covered by the IRAS 12 $\mu$m aperture are NGC 2992, and A1409-65. In the cases of NGC 3256 (also see Norris & Forbes, 1995), NGC 5253 and NGC 6221 a

[15]For the continuum 'luminosities' we use $4\pi D^2 \nu F_\nu = 4\pi D^2 \lambda F_\lambda$, where ($\nu$, $\lambda$) are the actual (frequency, wavelength) of the observation. For distances ($D$) in units of Mpc, and $F_\lambda$ in $10^{-17}$ W cm$^{-2}$ $\mu$m$^{-1}$ this means that $L_{2.1\,\mu m} = 2.51 \times 10^{33} F_{2.1\,\mu m} D^2$, with $L_{2.1\,\mu m}$ in Watt (W).

[16]The 2.1 $\mu$m continuum luminosity can be converted to the absolute K-band (@2.2 $\mu$m) magnitude (e.g., Rieke et al., 1990), which corresponds to the observed K-magnitude scaled to a distance of 10 pc. For a typical H − K = 0.4 mag (e.g., Devereux, 1989), we find $F_{2.2\,\mu m}/F_{2.1\,\mu m} = 0.89$. With $F_{K=0.0} = 4.12 \times 10^{-14}$ W cm$^{-2}$ $\mu$m$^{-1}$ (Koornneef, 1983a,b), it follows that $M_K = -2.5 \log L_{2.1\,\mu m} + 67.66$ (see Fig. 5).

[17]$L_{21\,cm} = 1.71 \times 10^{26} F_{1.4\,GHz} D^2$ [W]; $F_\nu$ in mJy – $L_{12\,\mu m} = 2.99 \times 10^{33} F_{12\,\mu m} D^2$ [W]; $F_\nu$ in Jy – $L_{6\,cm} = 5.98 \times 10^{26} F_{5\,GHz} D^2$ [W]; $F_\nu$ in mJy.

large fraction, of order 50%, of the disk is covered. However, for NGC 2992, A1409-65 & NGC 3256, Table 1 shows rather high compactness ratios. This suggests that only the 12 $\mu$m luminosities for NGC 5253 & NGC 6221 should be considered with caution, as they may not be representative for the mid-infrared luminosity of the galaxy's central region.

Radio continuum flux densities of the sample galaxy centers and nuclei were gathered from the literature (Table 7). Generally, the extent of the central radio continuum source is sufficiently small to make a comparison with the $H_2$ emission meaningful. We find that that the three luminosities $L_{1-0\,S(1)}$, $L_{12\,\mu m}$, and $L_{21\,cm}$ are fairly well correlated, although compared to the sample as a whole NGC 6240 has a rather high 1–0 S(1) luminosity, while NGC 4945 has a low 12 $\mu$m luminosity. Power law fits to the data, excluding those for NGC 6240, yield the following relations (in order of decreasing significance):

$$L_{1-0\,S(1)} = (14.3\pm3)\times L_{21\,cm}^{1.00\pm0.1}$$

$$L_{2.1\,\mu m} = (0.35\pm0.1)\times L_{12\,\mu m}^{1.24\pm0.15}$$

$$L_{1-0\,S(1)} = (0.74\pm0.2)\times L_{12\,\mu m}^{1.37\pm0.2}$$

$$L_{12\,\mu m} = (6.7\pm2)\times L_{21\,cm}^{0.63\pm0.3},$$

with $L_{1-0\,S(1)}$ & $L_{21\,cm}$ in units of $10^{32}$ W, and $L_{2.1\,\mu m}$ & $L_{12\,\mu m}$ in units of $10^{36}$ W.

The relation between $L_{1-0\,S(1)}$ and $L_{21\,cm}$ (Fig. 6) is particularly meaningful because both quantities refer to very similar parts of the observed galaxies. While the $L_{1-0\,S(1)}/L_{21\,cm}$ ratio shows no general trend with luminosity, some galaxies are sufficiently off the mean relation to deserve further scrutiny. In particular, NGC 253, NGC 2992, & NGC 4945 are characterized by a relatively low $L_{1-0\,S(1)}/L_{21\,cm}$ ratio, while NGC 3079, NGC 5128 (Cen A), NGC 5643, & NGC 6240 show high values for $L_{1-0\,S(1)}/L_{21\,cm}$. As $A_{2.1\,\mu m} = 1\pm1$ mag is a typical value for the 2.1 $\mu$m extinction of galaxy nuclei (the 21 cm fluxes are, of course, not affected by extinction), the observed spread around the mean relation could, at least partly, be due to extinction effects. Recently (Pérez-Olea & Colina, 1995), various evolutionary models of the radio emission in compact starbursts have become available. However, matching these models to our observational parameter space is a challenge that is beyond the scope of the current paper.

The relations involving $L_{12\,\mu m}$ all show exponents that differ significantly from unity in the sense that with increasing overall luminosity, $L_{12\,\mu m}$ increases *slower* than the other values. As in many brightness limited samples, the distances of the galaxies in our set are positively correlated with luminosity, with the result that the fixed size IRAS 12 $\mu$m aperture samples a larger linear area in the more distant & more luminous systems. If contributions from the galactic disks to the observed 12 $\mu$m fluxes were important, this aperture effect would tend to cause $L_{12\,\mu m}$ to increase *faster* than $L_{1-0\,S(1)}$, $L_{21\,cm}$ &

Table 8
Luminosities[a] of galaxy centers

| Galaxy | $D$ Mpc | $L_{1-0S(1)}$ $10^{32}$ W | $L_{21\,cm}$ $10^{32}$ W | $L_{12\,\mu m}$ $10^{36}$ W | $L_{2.1\,\mu m}$ $10^{36}$ W |
|---|---|---|---|---|---|
| NGC 253 | 2.5 | 0.09 | 0.028 | 0.38 | 0.03 |
| NGC1068 | 18 | 6.8 | 0.94 | 37 | – |
| NGC1365 | 21 | 4.0 | 0.34 | 4.2 | 5.5 |
| NGC1808 | 11 | 1.4 | 0.09 | 1.5 | 1.05 |
| NGC2992 | 28 | 1.7 | 0.36 | 1.4 | 1.15 |
| NGC3079 | 16 | 3.4 | 0.07 | 0.95 | 0.32 |
| NGC3256 | 37 | 13 | 1.4 | 13 | 2.5 |
| NGC4945 | 6.7 | 1.6 | 0.27 | 0.49 | 0.21 |
| NGC5128 | 3 | 0.07 | 0.0017 | 0.30 | 0.06 |
| NGC5236 | 3.7 | 0.08 | 0.010 | 0.19 | 0.04 |
| NGC5253 | 3.5 | 0.026 | 0.0015 | 0.095 | – |
| A1409-65 | 4 | 0.44 | 0.022 | 0.90 | 0.21 |
| NGC5643 | 16 | 1.3 | 0.015 | 0.66 | 0.36 |
| NGC6221 | 20 | 2.2 | 0.13 | 1.8 | 1.25 |
| NGC6240 | 100 | 323 | 3.9 | 17 | 8.6 |
| NGC6300 | 15 | 0.46 | 0.023 | 0.50 | 0.14 |
| NGC7552 | 20 | 3.5 | 0.15 | 3.6 | 1.2 |
| mean[b] | 10 | 0.88 | 0.06 | 1.1 | 0.36 |

Notes: [a] continuum luminosities defined as $4\pi D^2\nu F_\nu = 4\pi D^2\lambda F_\lambda$; [b] geometric mean, not including NGC 6240.

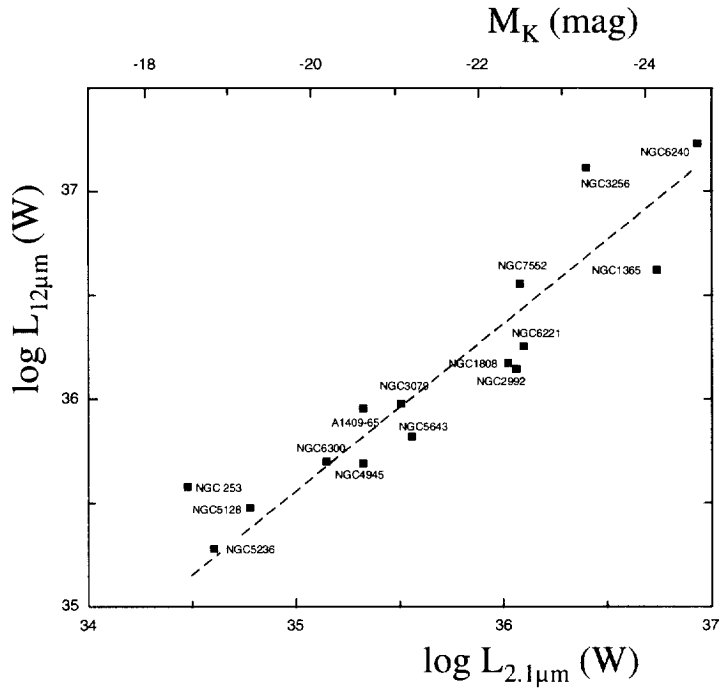


Fig. 5. We show the IRAS 12 $\mu$m continuum luminosities plotted against our 2.1 $\mu$m values. The observed behaviour is consistent with models in which the 2.1 $\mu$m fluxes are representative for the embedded stellar population, while the 12 $\mu$m fluxes are due to reprocessed starlight. This result can be compared with a study by Devereux (1989), who obtained data on the central 2.2 $\mu$m and 10 $\mu$m luminosities of a large sample of nearby spiral galaxies. The *upper envelope* of that dataset (his Fig. 2) matches our fitted line closely. In both cases, the slope deviates from unity in the direction expected if the reprocessing efficiency were somewhat smaller at high overall luminosities. Spiral galaxies without conspicuous nuclear activity have 12 $\mu$m luminosities up to several orders of magnitude fainter for the same 2.1 $\mu$m luminosity. The systems in the upper right hand corner, i.e. with observed (not corrected for reddening) K-magnitudes brighter than approximately $-23$ (see upper scale) do not have 'inactive' counterparts in the Devereux sample, and tend to be merger candidates (e.g., NGC 6240, NGC 3256).

$L_{2.1\ \mu m}$ with increasing overall luminosity. The fact that this is not observed supports our conjecture (also see Section 1) that the 12 $\mu$m fluxes are predominantly due to the nuclear regions, as already surmised from the compactness values of Table 1.

By comparison with the FIR-radio relation for radio-quiet active galaxies (e.g., Colina & Pérez-Olea, 1995), which refers to the infrared wavelength

Table 9
Slope[a] and (correlation coefficient)

| | $L_{1-0\,S(1)}$ | $L_{21\,cm}$ | $L_{12\mu m}$ | $L_{2.1\mu m}$ | $d_{H_2}$ |
|---|---|---|---|---|---|
| $L_{1-0\,S(1)}$ | ♦ | | | | |
| $L_{21\,cm}$ | 1.00(0.90) | ♦ | | | |
| $L_{12\mu m}$ | 0.73(0.87) | 0.63(0.84) | ♦ | | |
| $L_{2.1\mu m}$ | 0.88(0.89) | 0.68(0.77) | 1.24(0.90) | ♦ | |
| $d_{H_2}$ | 0.49(0.93) | 0.39(0.82) | 0.71(0.92) | 0.54(0.94) | ♦ |

Note: [a] Power law fits to the quantities shown, excluding NGC 6240; for example: $d_{H_2} \propto L_{1-0\,S(1)}^{0.49}$.

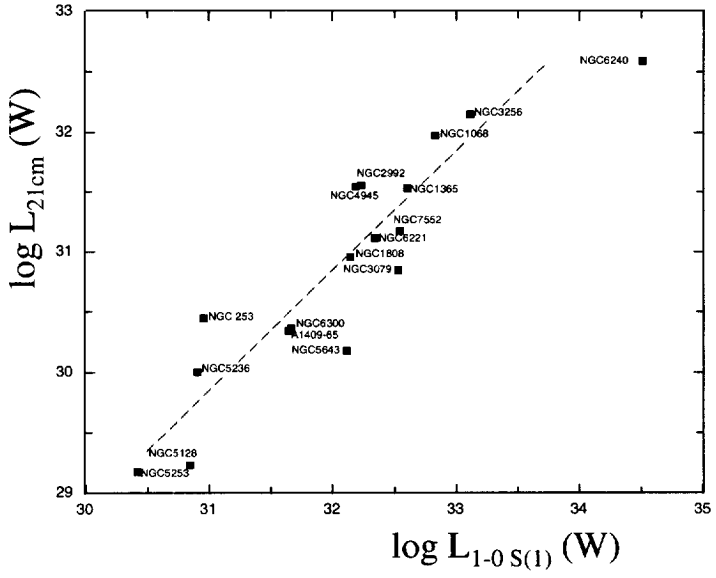


Fig. 6. The nuclear 21 cm *continuum* luminosities are plotted against the $H_2$ S(1) values. The high degree of correlation over a large range in luminosity suggests that the outflow mechanism responsible for the shock excitation of the molecular hydrogen is linked to the source of the nonthermal radio continuum. If the relativistic electrons responsible for the bulk of the 21 cm fluxes are injected in the central region of the galaxy by supernovae, those nuclei off the average relation in the direction of the upper left hand corner of this diagram would have the highest SN-rates. However, one of the findings of the present paper (Section 4.2) is that extinction at 2.1 $\mu$m is not negligible. As dereddening will move the data-points to the right and because galaxies like NGC 4945 & NGC 253 are argued to have fairly substantial extinction, while NGC 6240 does not, part of the scatter in the current diagram is probably due to extinction.

range *beyond* 12 $\mu$m, we find that the ratio of $L_{12\,\mu m}$/FIR decreases with increasing luminosity. Qualitatively, and quite reasonably, this suggests that fraction of hot dust is relatively large in the more compact systems.

### 4.4. Central luminosities and $H_2$ extent

In an attempt to constrain the conditions in the centres of the sample galaxies, we have investigated the relation between the size of the $H_2$ emitting region and the various luminosities.

Firstly, we correlate the $H_2$ 1–0 S(1) line luminosity $L_{1-0\,S(1)}$ with its extent $d_{H_2}$ (Fig. 7) and derive (Table 9):

$$L_{1-0\,S(1)} = (10.0\pm2)d_{H_2}^{2.03\pm0.2},$$

where $d_{H_2}$ is in kpc and $L_{1-0\,S(1)}$ is in units of $10^{32}$ W. This relation implies that the $H_2$ surface brightness $L_{1-0\,S(1)}/(d_{H_2})^2$ is approximately the same for the galaxies in the sample (cf. Table 6), and that the variations in $H_2$ luminosity (which cover a range of almost three orders of magnitude) are primarily due to different sizes of the emitting region, but are not strongly influenced by source to source variation in the internal extinction or the actual excitation mechanism (with NGC 6240 as an important exception.) The characteristic value for the observed (i.e., not de-reddened) $H_2$ surface brightness of our infrared brightness selected galaxy sample is $\sigma_{1-0\,S(1)} = 1.7\pm0.5\times10^{-4}$ erg cm$^{-2}$ s$^{-1}$ ster$^{-1}$. This can be compared with a value of $\sigma_{1-0\,S(1)} \approx 5\times10^{-6}$ erg cm$^{-2}$ s$^{-1}$ ster$^{-1}$, which was recently observed for the (non-active) nuclear region of our Galaxy by Pak et al. (1996).

We also correlated the $H_2$ extent ($d_{H_2}$) with the 21 cm radio continuum luminosity ($L_{21\,cm}$; also ex-

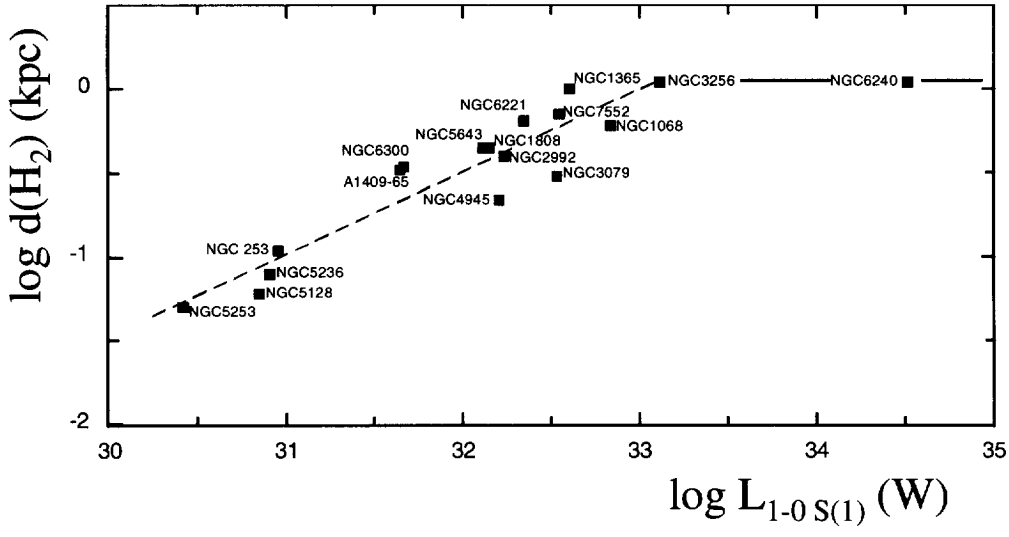


Fig. 7. The observed sizes of the $H_2$ emitting regions for 17 galaxy centers are plotted against the luminosities emitted in the $H_2$ 1–0 S(1) line. The slope of our linear fit (which excluded NGC 6240) is consistent with a simple model in which all nuclear regions have approximately the same surface brightness ($\sigma = 1.7\pm0.5\times10^{-4}$ erg cm$^{-2}$ s$^{-1}$ ster$^{-1}$) in the 1–0 S(1) line, but differ in size. We note that none of the emitting regions is significantly larger than 1 kpc. Perhaps coincidentally, this is also the value at which the size distribution function for supergiant shells in local galaxies terminates (e.g., Bomans et al., 1994).

pressed in units of $10^{32}$ W.) We cannot easily conceive of a physical process that would lead to a dependence of $L_{21\,\mathrm{cm}}$ on $d_{H_2}$, but instead pursue the possibility of the converse dependence. We find (excluding NGC 6240) a significant relationship (Table 9):

$$d_{H_2} = (0.89\pm0.3)\times L_{21\,\mathrm{cm}}^{0.39\pm0.08}.$$

Some conceptual simplification can be achieved by assuming that the *actual* value of the exponent is 0.5, rather than the *observed* 0.39±0.08. We can then rewrite the above relationship (with $d_{H_2}$ in kpc and $L_{21\,\mathrm{cm}}$ in units of $10^{32}$ W):

$$d_{H_2} = (1.22\pm0.4)\times L_{21\,\mathrm{cm}}^{0.5},$$

which is identical to:

$$r_{H_2} = (1.88\pm0.5)10^5\times L_{21\,\mathrm{cm}}^{0.5},$$

except that $r_{H_2}$ is now in cm and $L_{21\,\mathrm{cm}}$ in W. This equation, in combination with a simplified morphology consisting of a radially thin $H_2$ emitting shell wrapped around the nucleus that is the source of the $H_2$ excitation as well as the 21 cm radiocontinuum flux, leads to the unanticipated conclusion that the $H_2$ emission occurs at that distance from the nucleus where the incident 21 cm flux equals $(2.25\pm0.6)10^{-8}$ W m$^{-2}$ independent of the actual central luminosity.

Also, the 12 $\mu$m luminosity shows a very significant correlation with $d_{H_2}$:

$$L_{12\,\mu\mathrm{m}} = (5.2\pm3)d_{H_2}^{1.41\pm0.4}$$

where $L_{12\,\mu\mathrm{m}}$ is in units of $10^{36}$ W. In order to interpret this result, we have also investigated the behaviour of both the ratio $L_{1-0\,S(1)}/L_{12\,\mu\mathrm{m}}$ and $L_{12\,\mu\mathrm{m}}/L_{21\,\mathrm{cm}}$ as a function of $d_{H_2}$. Both ratios show considerable scatter with respect to $d_{H_2}$, but with this proviso we find the following correlations:

$$L_{1-0\,S(1)}/L_{12\,\mu\mathrm{m}} = (1.6\pm0.8)d_{H2}^{0.55\pm0.15}$$

$$L_{12\,\mu\mathrm{m}}/L_{21\,\mathrm{cm}} = (9.6\pm4.2)d_{H2}^{-0.54\pm0.15}.$$

We note that these relations are not influenced by the two galaxies whose 12 $\mu$m flux may include significant disk emission (Section 4.3). As expected, the ratio $L_{1-0\,S(1)}/L_{21\,cm}$ shows a large scatter around a constant value independent of $d_{H2}$. What we thus see is that as $L_{21\,cm}$, and consequently the size of the $H_2$ emitting zone increase, both $L_{1-0\,S(1)}$ and $L_{12\,\mu m}$ increase, but the latter much slower than the former.

Finally, we have compared $L_{1-0\,S(1)}$ and $L_{CO}$ luminosities. The CO luminosities are defined as $L_{CO} = \pi I_{CO} R^2$ [K km s$^{-1}$ kpc$^2$], where $2R$ is the linear diameter of the SEST 40 arcsec CO observing beam (Israel et al. (1995); Israel & Baas, in preparation) at the assumed galaxy distance. We find:

$$L_{1-0\,S(1)} = 3.5 \times 10^{-3} L_{CO}$$

with $L_{1-0\,S(1)}$ in units of $10^{32}$ W and $L_{CO}$ in units of K km s$^{-1}$ kpc$^2$. Although the distribution of CO in the sample galaxies was not mapped, the good correlation between $L_{1-0\,S(1)}$ and $L_{CO}$ suggest that in the majority of galaxies the bulk of the central CO emission originates on scales less than 40 arcsec, corresponding to 0.7 kpc for the nearest galaxies in the sample, and to a few kpc for the more distant ones. Note that for an assumed average 2.1 $\mu$m extinction $A_{2.1\,\mu m} = 1$ mag (Section 4.2), the above relation becomes $L_{1-0\,S(1)} = 0.9 \times 10^{-2} L_{CO}$. Physically, the interpretation of this result is most straightforward if an energy source *within* the $H_2$ emitting volume – an option we discuss in Section 4.5.2 – is also responsible for the heating of the CO.

A more detailed comparison between $H_2$ & CO emissions makes for a challenging, and potentially rewarding, line of research but is beyond the scope of the present paper. Additional high spatial resolution measurements in multiple CO-transitions (e.g., *IRAM*, Owens Valley) are needed, as well as $H_2$ data in various rotational-vibrational transitions covering a range in excitation temperatures (which can be obtained with the *Short Wavelength Spectrograph* on the *Infrared Space Observatory*).

### 4.5. Structure of circumnuclear $H_2$ zones

Although the data discussed so far generally do not resolve the central emission, they nevertheless allow us to draw some conclusions on the structure of the central regions in the galaxies studied. The relevant points are:

i) the observed $H_2$ is shock-excited;

ii) the extent of $H_2$ is proportional to the square root of the 21 cm radio continuum luminosity;

iii) the central $H_2$ luminosity is proportional to the square of the $H_2$ extent;

iv) the strength of the central $H_2$ luminosity is proportional to the central CO emission;

v) the near-infrared 12 $\mu$m luminosity increases with $H_2$ radius significantly less rapidly than the $H_2$ luminosity.

These items suggest that a) both CO and 12 $\mu$m emission are concentrated on (sub)kiloparsec scales and b) that the same processes that lead to 21 cm continuum emission also dominate the $H_2$ emission from the centers of the sample galaxies.

With respect to the location of the source of energy in relation to the gaseous emitting regions, we will now discuss two simplified geometries. In the first case, we place the emitting gas *intermingled* with (mass losing-)stars and SNe in an extended circumnuclear zone. Alternatively, the source of energy may be fairly compact (i.e., $\lesssim$ 100pc) stellar (or possibly non-stellar) nucleus that is losing mass at such a rate that molecular material can only exist *around* the nucleus. or a more extended. In either case, we assume that the observed 21 cm radio continuum emission is a measure for the total energy output of either nucleus or circumnuclear zone. In effect, this supposes that the galaxies studied have similar central continuum spectra.

#### 4.5.1. Supernovae in a starburst disk

Points i), ii) and iii) are compatible with either situation. If an extended circumnuclear SNR zone provides the energy, we expect a disk filled throughout with shocked $H_2$ regions. Since the number of SNR's will be proportional to the disk surface area, both $L_{1-0\,S(1)}$ and $L_{21\,cm}$ will be proportional to $dN_{SN}/dt$ and hence on $d^2_{H_2}$. The dependence of both $L_{1-0\,S(1)}$ and $L_{21\,cm}$ on $dN_{SN}/dt$ provides a check on

this hypothesis. Following the arguments by Rotaciuc et al. (1991), we may estimate $dN_{SN}/dt = 5 \times 10^{-34} L_{1-0\,S(1)}$ with $dN_{SN}/dt$ expressed as the number of supernovae per year and $L_{1-0\,S(1)}$ is expressed in Watts. This assumes a blast wave energy of $10^{44}$ W s per supernova. Likewise, by assuming a nonthermal radio spectral index $\alpha = -0.7$ we may relate the supernova rate to the nonthermal radio luminosity by $dN_{SN}/dt = 2\ 10^{-32} L_{21\,cm}$, thus *predicting* a ratio $L_{1-0\,S(1)}/L_{21\,cm} = 40$.

The variation in the *observed* ratios – while substantial – is much smaller than the range in luminosity (see Fig. 6 & Table 8), and a typical value is $L_{1-0\,S(1)}/L_{21\,cm} = 15$. As the two highly obscured starburst galaxies NGC 253 and NGC 4945 have an excess 21 cm relative to the mean relationship, while NGC 5643 & NGC 6240 have $L_{1-0\,S(1)}/L_{21\,cm}$ ratios much closer to the predicted value, it is likely that the scatter in the observed relationship would decrease if the $H_2$ 1–0 S(1) data were appropriately dereddened. This would then also move the observed ratio closer to the predicted ratio.

Because of the good correlation between $L_{21\,cm}$ and $d^2_{H_2}$, the *surface density* of supernovae must be very similar in the sample galaxies, even though the supernova *rates* predicted by taking the means of $L_{1-0\,S(1)}$ and $L_{21\,cm}$ from Table 8 vary greatly from about 0.1–1.0 $yr^{-1}$ for NGC 1068, 1365, 1808, 2992, 3079, 4945, 6221 and 7552. Supernova rates an order of magnitude lower would be predicted for NGC 253, Cen A, M83, A1409-65 (Circinus), NGC 5643 and NGC 6300. NGC 5253 would have a rate of only 0.002 $yr^{-1}$, another order of magnitude lower.

Thus, the idea that (a large number of) supernova remnants originating from a recent starburst contribute to both the observed 21 cm radio continuum emission and the excitation of the observed $H_2$ is qualitatively consistent with the observed $L_{1-0\,S(1)}/L_{21\,cm}$ ratios. However, in the embedded model, young hot stars associated with the starburst would produce HII regions within the molecular regions, and the observed $H_2$ line ratios would be expected to be fluorescent which is not observed. Also, the fact that significant energy may be injected by mass losing stars, and those cases where a non-thermal pointlike nucleus contributes to the radio emission and the mechanical energy cannot be readily accommodated in the embedded model[18].

There is also considerable geometrical evidence for deviations from the simplified filled disk model: several galaxies from our sample, such as NGC 253, NGC 1365, NGC 3079, NGC 4945, A1409-65 (Circinus), NGC 4945, NGC 7552 and especially NGC 5128 (Cen A) show circumnuclear tori or disks *with a central hole*, i.e. not homogeneously filled disks (Carlstrom et al., 1990; Harnett et al., 1990; Whiteoak et al., 1990; Bergman et al., 1992; Israel, 1992; Koornneef, 1993; Israel et al., 1990, 1991).

*4.5.2. Circumnuclear disk with a hole*

Noting that the circumnuclear disk of NGC 5128 (Cen A) is much larger in CO than in excited $H_2$, Israel et al. (1990, 1991) proposed that the observed $H_2$ is the excited inner edge of a circumnuclear disk with a central hole. This hole may be caused by an outflow from a compact nucleus, which would also produce a double radio lobe galaxy, or by strong winds from massive stars and supernova blasts following a nuclear starburst. Such a superwind model was put forward by Heckman et al. (1990) to explain optical spectroscopic observations of strongly far-infrared emitting galaxies (FIRG's). Their sample has some overlap with the galaxies discussed in this paper: it contains NGC 253, NGC 3079, NGC 3256 and NGC 4945. This situation may apply not only to NGC 3079 (Hawarden et al., 1995), NGC 4945 (Bergman et al., 1992; Koornneef, 1993) and the archetypical starburst galaxy M82, but also to A1409-65 (Circinus) (Harnett et al., 1990) and NGC 1808 (Saikia et al., 1990; Aalto et al., 1994). Given the evidence cited in Section 4.5.1, it is likely that the majority of galaxies observed in our sample contain a circumnuclear disk with a central hole,

[18] For NGC 1068, Rotaciuc et al. (1991) explicitly argue that the morphology and flux ratios of the radio and $H_2$ structures, respectively, are not compatible with a common, i.e. supernova, excitation mechanism.

where the $H_2$ emission[19] traces the inner edge of the molecular disk, rather than the outer edge of a completely filled disk.

This explanation is consistent with the generally low ratio of Br$\gamma$ to 1–0 S(1) $H_2$ emission (Moorwood & Oliva, 1990; Israel et al., 1990; Koornneef, 1993) which would be more difficult to explain in the case of a filled disk excited by starburst events only. The good correlation between $L_{1-0\,S(1)}$ and $L_{CO}$ suggests that inner and outer diameters of the torus scale reasonably well, but may also be due to a strong density gradient in the CO disk. The dependence of diameter $d_{H_2}$ on $L_{21\,cm}^{0.5}$ is very similar to the result found by Heckman et al. (1990) (e.g., their Fig. 17) that the radius $r_{n100}$ where ram pressure dominates scales as $L_{IR}^{0.5}$. If both $L_{21\,cm}$ and $L_{IR}$ scale with total mechanical luminosity, it confirms that the inner edge of the circumnuclear disk occurs at constant pressure. The relatively slow increase of $L_{12\,\mu m}$ with cavity size $d_{H_2}$ suggests that in contrast to the $H_2$ emission which takes place in a very thin 'skin' the mid-infrared emission originates in a region with a finite but more or less constant depth in the inner circumnuclear disk.

There is some evidence that the remaining molecular gas could be concentrated around the inner–inner Lindblad resonance, and that (secondary) star-formation might occur there. In two galaxies that are not observed by us, NGC 7469 (Genzel et al., 1995), and NGC 3504 (Kenney et al., 1993), the $H_2$ emission could then be associated with starforming circumnuclear rings. For the reasons given earlier, we do not consider it likely that this geometry applies for a significant fraction of the galaxies in our sample.

## 5. Concluding remarks

One often-remarked-on finding in active galaxy research is the existence of a good correlation between observables from widely separated spectral regimes, and with rather different excitation mechanisms. We have studied a sample of nearby southern IRAS galaxies with infrared excesses, and find that our sample corresponds with the upper envelope of the 2.2 versus 10 $\mu$m diagram of the spiral galaxy sample studied by Devereux (1989)[20]. We find a number of correlations which are quite independent of the actual classification of the galactic nucleus (e.g., Liner, Seyfert, or starburst), and which hold over a large range in luminosity. This correlation study is presented in Section 4.3 Section 4.4, and covers a number of parameters: the size of the 1–0 S(1) $H_2$ emitting regions as well as the luminosity emitted in the principal 1–0 S(1) transition, and the continuum luminosities at wavelengths of 2.1 $\mu$m, 12 $\mu$m, & 21 cm. These parameters share the property that they are minimally affected by the dust commonly present in galaxy nuclei, and avoid the complex analysis and interpretation of optical observations (e.g., Veilleux et al., 1995).

Our main finding is that the various luminosities and the linear extent of the inner active region in galaxy centers are closely related, with little dependence on the specific type of nuclear activity. In fact, while we initially prepared plots of each of the correlations discussed in the present paper with different symbols for the various nuclear classifications (i.e., starburst, Liner, Seyfert 2, ...), in none of the diagrams a clear separation of the various types was achieved. We therefore use only a single set of symbols in the present version of the diagrams, and refrain from tabulating the nuclear types. This seems especially appropriate given the ongoing, and often rather heated, discussions on the nuclear types of many of the galaxies in our sample.

We also find that the shock-mechanism dominates the excitation of the observed $H_2$, but cannot unambiguously discriminate between mass losing (super-)giants & Wolf-Rayet stars, supernovae – or

[19]For $H_2$ emission lines arising from lower levels than the 1–0 S(1) line, the emitting region would be expected to be larger. But even for the 0–0 S(0) line at 28.2 $\mu$m, the most effective excitation temperature is in the order of 500 K. Consequently, the CO disk will be larger than the $H_2$ disk in all rotational-vibrational emission lines.

[20]Devereux (1989) expresses the 2.2 $\mu$m luminosities in solar units. For an absolute solar magnitude at 2.2 $\mu$m of $M_K = +3.39$, $\log L_{2.2\,\mu m}/L_\odot = (-M_K + 3.39)/2.5$, which is equivalent to $\log L_{2.2\,\mu m}/L_\odot = \log L_{2.1\,\mu m}$ [W] − 25.71.

even outflow from accreting non-thermal nuclei – as the source of the kinetic energy. The absence of a substantial fluorescent component in most nuclei can be understood to imply that central starbursts tend to be instantaneous as this has the consequence that there are only hot luminous stars available during a small fraction of the total lifetime of the burst. Several nuclei have thus been characterized as 'postburst'. The $H_2$ excitation mechanisms for the systems in our sample with UV bright Seyfert nuclei (e.g., NGC 1365 & NGC 2992) remains to be determined as we do not have reliable $H_2$ line ratios for these galaxies.

We did not explicitly consider X-ray excitation. X-rays (which can originate from nuclear accretion disks, as well as from starburst-related phenomena) are unlikely to be an important source of excitation of the molecular hydrogen (e.g., Mouri, 1994). Among other reasons, the predicted $H_2$ line ratios (Black & van Dishoeck, 1987; Gredel & Dalgarno, 1995) are probably not consistent with the observed values (see also Hawarden et al., 1995).

Our findings are in line with the results obtained in other investigations of such objects. For instance, a recent spectroscopic study of 200 luminous northern IRAS galaxies led Veilleux et al. (1995) to suggest that large-scale nuclear winds are indeed common in luminous IRAS galaxies. Circumnuclear starburst activity is found to be common in luminous infrared galaxies *regardless* of the nuclear spectral type. Moreover, most of the Liner emission from these galaxies is produced through shock ionization rather than photoionization. Similarly, the good correlation between [FeII] 1.64 $\mu$m and 6 cm radio continuum emission from the nuclei of active galaxies, established by Forbes & Ward (1993), indicates that *again irrespective* of nuclear type, the same shock mechanism is responsible for the strong emission from these nuclei.

Thus, the results obtained by Forbes & Ward (1993), by Veilleux et al. (1995), and those presented here in Section 4.3 Section 4.4 all point squarely at the dominating influence of strong winds from the galaxy nucleus or its immediate surroundings. The overall characteristics of the inner parts of galaxies are dominated by the mechanics of these winds, irrespective of the precise origin of the winds (nucleus or circumnuclear SNR's). The mechanical energy input determines the emerging luminosities and the inner cavity sizes. The origin of the energy input may be nuclear winds from an AGN, a (circum)nuclear starburst or both. The balance between these mechanisms may depend on the epoch of observation, as the inward transport of gaseous material, the degree of activity of the nucleus, and the occurrence of circumnuclear starbursts are probably all related. The intimate relationship between active galaxy nuclei and circumnuclear starbursts makes it difficult to separate the effects of these two phenomena in area-integrated observations of both line and continuum emission from centers of galaxies.

This may be illustrated by a final comment. As the size of the inner, presumably dustfree, cavity decreases with decreasing (circum)nuclear luminosity, low-luminosity AGN's should on average suffer significantly higher extinctions than high-luminosity AGN's. The combined effect of lower intrinsic luminosity and higher extinction rapidly decreases the likelihood of identifying such AGN's. In addition, the presence of other luminous sources in the central regions of such galaxies will only serve to further decrease the contrast of an AGN to its surroundings.

Given the difficulties of establishing the presence of AGN's, it is possible that the fraction of luminous galaxies containing an AGN is currently underestimated. Veilleux et al. (1995) report that the fraction of luminous IRAS galaxies with identifiable AGN spectra and the fraction of Seyfert galaxies among the AGN increases with (infrared) luminosity. Infrared coronal lines appear to provide very promising diagnostics (e.g., Oliva et al., 1994) but the database of published observations is still limited and must be enlarged. The search for unambiguous symptoms for such nuclear characteristics as: the presence of an AGN, the supernova-rate, the star-formation rate and the nuclear mass loss rates will continue. Infrared emission lines from a range of species and ionization stages will be particularly helpful in determining the physical conditions in the optically-obscured interiors of these objects, to discriminate between stellar

and non-thermal processes as the ultimate source of the luminosity, and to reliably determine the fraction of AGN's among (lower-luminosity) IRAS galaxies.

## Acknowledgments

It is a pleasure to thank Drs. P. Barthel, M. Dahlem and J.M. van der Hulst for helpful comments.

## References

Aalto, S., Booth, R.S., Black, J.H., Koribalski, B., & Wielebinski, R., 1994, A&A, 286, 365.
Ables, J.G., Forster, J.R., Manchester, R.N., Rayner, P.T., Whiteoak, J.B., Mathewson, D.S., Kalnajs, A.J., Peters, W.L., & Wehner, H., 1987, MNRAS, 226, 157.
Agüero, E.L. & Carranza, G.J., 1986, Ap&SS, 121, 403.
Allen, D.A. & Burton, M.G., 1993, Natur, 363, 54.
Baas, F., Israel, F.P., & Koornneef, J., 1994, A&A, 284, 403.
Bergman, P., Aalto, S., Black, J.H., & Rydbeck, G., 1992, A&A, 265, 403.
Black, J.H. & van Dishoeck, E.F., 1987, ApJ, 322, 412.
Bomans, D.J., 1994, Doktoral Dissertation, Bonn, Deutschland.
Bosma, A., Goss, W.M., & Wellington, K.J., 1983, A&AS, 54, 387.
Brand, P.W.J.L., Toner, M.P., Geballe, T.R., Webster, A.S., Williams, P.M., & Burton, M.G., 1989, MNRAS, 236, 929.
Cameron, M., Storey, J.W.V., Rotaciuc, V., Genzel, R., Verstraete, L., Drapatz, S., Siebenmorgen R., & Lee, T.J., 1993, ApJ, 419, 136.
Carlstrom, J.E., Jackson, J.E., Ho, P.T.P., & Turner, J.L., 1990, in: The Interstellar Medium in Galaxies: Summaries of Contributed Papers, eds. H.J. Hollenbach & H.A. Thronson, NASA CP 3084, p. 337.
Colina, L. & Pérez-Olea, D.E., 1995, MNRAS, 277, 845.
Condon, J.J. 1987, ApJS, 65, 485.
Condon, J.J., Gordon, M.A., Gisler. G., & Puschell, J.J., 1982, ApJ, 252, 102.
Dahlem, M., Hartner, G.D., & Junkes, N., 1994, ApJ, 432, 598.
de Vaucouleurs, G., 1964, ApJ, 139, 899.
Devereux, N.A., 1989, ApJ, 346, 126.
Doyon, R., Wright, G.S., & Joseph, R.D., 1994, ApJ, 421, 115.
Draine, B.T., Roberge, W.G., & Dalgarno, A., 1983, ApJ, 264, 485.
Forbes, D.A., 1993, Ap&SS, 205, 37.
Forbes, D.A., Ward, M.J., Rotaciuc, V., Blietz, M., Genzel, R., Drapatz, S. van der Werf, P., & Krabbe, A., 1993, ApJ, 406, L11.
Forbes, D.A. & Ward, M.J., 1993, ApJ, 416, 150.
Frogel, J.A., Gregory, B., Kawara, K., Laney, D., Phillips, M.M., Terndrup, D., Vrba, F., & Whitford, A.E., 1987, ApJ, 315, L129.
Genzel, R., Weitzel, L., Tacconi-Garman, L.E., Blietz, M., Cameron, M., Krabbe, A., Lutz, D., & Sternberg, A., 1995, ApJ, 444, 129.
Giuricin, G., Tamburine, L., Mardirossian, F., Mezetti & M., Monaco, P., 1994, ApJ, 427, 202.
Goldader, J.D., Joseph, R.D., Doyon, R., & Sanders, D.B., 1995, ApJ, 444, 97.
Gredel, R., & Dalgarno, A., 1995, ApJ, 446, 852.
Harnett, J.I., 1987, MNRAS, 227, 887.
Harnett, J.I., Whiteoak J.B., Reynolds J.E., Gardner F.F., & Tzioumis A., 1990, MNRAS, 244, 130.
Harris, G.L.H., Hesser, J.R., Harris, H.C., & Curry, P.J., 1984, ApJ, 287, 175.
Hawarden, T.G., Israel, F.P., Geballe, T.R., & Wade, R., 1995, MNRAS, 276, 1197.
Heckman, T.M., Armus, L., & Miley, G.K., 1990, ApJS, 74, 833.
Hui, X., Ford, H.C., Ciardullo, R., & Jacoby, G.H., 1993, ApJ, 414, 463.
Israel, F.P. & Koornneef, J., 1988, A&A, 190, 21.
Israel, F.P. & Koornneef, J., 1991, A&A, 250, 475.
Israel, F.P., van Dishoeck, E.F., Baas, F., Koornneef, J., Black, J.H., & de Graauw, T., 1990, A&A, 227, 342.
Israel, F.P., van Dishoeck, E.F., Baas, F., de Graauw, T., & Phillips T.G., 1991, A&A, 245, L13.
Israel, F.P., 1992, A&A, 265, 487.
Israel, F.P., Tacconi, L.J., & Baas, F., 1995, A&A, 295, 599.
Kawara, K., Nishida, M., & Gregory, B., 1987, ApJ, 321, L35 (KNG).
Kawara, K., Nishida, M., & Taniguchi, Y., 1988, ApJ, 328, L41.
Kenney, J.D.P., Carlstrom, J.E., & Young, J.S., 1993, ApJ, 418, 687.
Kennicutt, R.C., 1994, in: Mass-Transfer Induced Activity in Galaxies, ed. I. Shlosman (Cambridge: Cambridge Univ. Press) p. 131.
Knapen, J.H., Beckman, J.E., Heller, C.H., Shlosman, I., & de Jong, R.S., 1995, ApJ, 454, 623.
Koornneef, J., 1983a, A&AS, 51, 489.
Koornneef, J., 1983b, A&A, 128, 84.
Koornneef, J., 1993, ApJ, 403, 581.
Kotilainen, J.K., Moorwood, A.F.M., Ward, M.J., & Forbes, D.A., 1995, A&A, in print.
Krabbe, A., Sternberg, A., & Genzel, R., 1994, ApJ, 425, 72.
Leitherer, C., Robert, C., & Drissen, L., 1992, ApJ, 401, 596.
Moorwood, A.F.M. & Oliva, E., 1988, A&A, 203, 278 (MO88).
Moorwood, A.F.M. & Oliva, E., 1989, in: Proc. of 22nd ESLAB Symposium on Infrared Spectroscopy in Astronomy, ed. B.H. Kaldeich (ESA SP290), 507.
Moorwood, A.F.M. & Oliva, E., 1990, A&A, 239, 78 (MO90).
Moorwood, A.F.M. & Origlia, L., 1991, in: Astrophysics with Infrared Arrays, ed. R. Elston (ASP Conf. Ser. 14) p. 85.

Moorwood, A.F.M. & Oliva, E., 1994, ApJ, 429, 602.
Moorwood, A.F.M., van der Werf, P.P., Kotilainen, J.K., Marconi, A., & Oliva, E., 1996, A&A, 308, L1.
Mouri, H., Taniguchi, Y., Kawara, K., & Nishida, M., 1989, ApJ, 346, L73.
Mouri, H., Kawara, K., Taniguchi, Y., & Nishida, M., 1990, ApJ, 356, L39.
Mouri, H., Nishida, M., Taniguchi, Y., & Kawara, K., 1990, ApJ, 360, 55.
Mouri, H., 1992, MNRAS, 257, 433.
Mouri, H. & Taniguchi, Y., 1992, ApJ, 386, 68.
Mouri, H., Kawara, K., & Taniguchi, 1993, ApJ, 406, 52.
Mouri, H., 1994, ApJ, 427, 777.
Muñoz-Tuñon, C., Vilchez, J.M., & Castañeda, H.O., 1993, A&A, 278, 364.
Neff, S.G., Fanelli, M.N., Roberts, L.J., O'Connell, R.W., Bohlin, R.C., Roberts, M.S., Smith, A.M., & Stecher, T.P., 1994, ApJ, 430, 545.
Norris, R.P., & Forbes, D.A., 1995, ApJ, 446, 594.
Norman, C.A., 1991, in: Massive Stars in Starbursts, eds. C. Leitherer, N.R. Walborn, T.M. Heckman & C.A. Norman (Cambridge: Cambridge Univ. Press), 271.
Oliva, E., Salvati, M., Moorwood, A.F.M., & Marconi, A., 1994, A&A, 288, 457.
Ondrechen, M.P., 1985, AJ, 90, 1474.
Pak, S., Jaffe, D.T., & Keller, L.D., 1996, ApJ, 457, L43.
Pérez-Olea, D.E. & Colina, L., 1995, MNRAS, 277, 857.
Piña, R.K., Jones, B., Puetter, R.C., & Stein, W.A., 1992, ApJ, 401, L75.
Prada, F., Manchado, A., Canzian, B., Peletier, R., McKeith, C.D. & Beckman, J.E., 1996, ApJ, 458, 537.
Puxley, P.J., Hawarden, T.G., & Mountain, C.M., 1988, MNRAS, 234, 29P (PHM).
Rotaciuc, V., Krabbe, A., Cameron, M., Drapatz, S., Genzel, R., Sternberg, A., & Storey, J.W.V., 1991, ApJ, 370, L23.
Rieke, G.H., Lebofsky, M.J., Thompson, R.I., Low, F.J., & Tokunaga, A.T., 1980, ApJ, 238, 24.
Saikia, D.J., Unger, S.W., Pedlar, A., Yates, G.J., Axon, D.J., Wolstencroft, R.D., Taylor, K., & Gyldenkerne K., 1990, MNRAS, 245, 397.
Sams, B.J., Genzel, R., Eckart, A., Tacconi-Garman, L., & Hofmann, R., 1994, ApJL, 430, 33.
Sandquist, A., Jorsaler, S., & Linblad, P.O., 1982, A&A, 110, 336.
Schreier, E.J., Burns, J.O., Feigelson, & E.D., 1981, ApJ, 251, 523.
Scoville, N.Z., Hall, D.N.B., Kleinmann, S.G., & Ridgway, S.T., 1982, ApJ, 253, 136.
Shull, J.M. & Hollenbach, D.J., 1978, ApJ, 220, 525.
Shull, J.M. & Draine, B.T., 1987, in: Interstellar processes; Proceedings of the Symposium, Grand Teton National Park, WY, July 1–7, 1986. Dordrecht, D. Reidel Publishing Co, p. 283-319..
Sternberg, A. & Dalgarno, A., 1989, ApJ, 338, 197.
Suchkov, A.A., Balsara, D.S., Heckman, T.M., & Leitherer, C., 1994, ApJ, 430, 511.
Thompson, R.I., Lebofsky, M.J., & Rieke, G.H., 1978, ApJ, 222, L49.
Tzioumis, A.K., 1987, Ph.D. Thesis, Univ. Sydney, Australia.
van der Werf, P., Genzel, R., Krabbe, A., Blietz, M., Drapatz, S., Ward, M.J., & Forbes, D.A., 1993, ApJ, 405, 522.
Veilleux, S., Kim, D.-C., Sanders, D.B., Mazzarella, J.M., & Soifer, B.T., 1995, ApJS, 98, 171.
Ward, M., Penston, M.V., Blades, J.C., & Turtle, A.J., 1980, MNRAS, 193, 563.
Whiteoak, J.B. & Bunton, J.D., 1985, Proc. ASAu, 6, 171.
Whiteoak, J.B., Dahlem, M., Wielebinski, R., & Harnett, J.I., 1990, A&A, 231, 25.
Whiteoak, J.B. & Wilson, 1990, MNRAS, 245, 665.
Wynn-Williams, C.G., Becklin, E.E., & Scoville, N.Z., 1985, ApJ, 297, 607.